

1

Improved Treatment of Dark Matter Capture in Compact Objects

Review capture in the Sun, move to what's needed for COs in general, then specify to WDs (ions + electrons) and NS (interacting baryons)

The capture rate of dark matter within celestial bodies is an essential quantity of interest throughout this work. In this chapter, we focus on building up the formalism of dark matter capture within compact objects derived in Refs. [1, 2], outlining how our results differs from the established formalism for capture in the Sun.

We note that the main results presented in this chapter are given for DM scattering from neutron targets, and was completed before the additional complications to the capture rate that arise baryons having strong self-interactions and a finite size were realised in Refs. [3, 4]. As such, these results serve to highlight the key features of the capture formalism we derive. The results of Refs. [3, 4] will be discussed in Chapter ??.

1.1 Dark Matter Capture in the Sun

Before jumping into the capture formalism relevant to compact objects, it will serve us well to review the formalism laid out by Gould for capture in the Sun [5, 6].

To begin, we consider the flux of dark matter particles that pass through a spherical shell a large distance R from the star, where the gravitational field is

negligible. For this, we need to know the distribution function of the relative velocity between the DM and the stellar constituents. The velocity distribution function will be spatially isotropic, and so for simplicity we will assume that the DM follows a Maxwell-Boltzmann distribution function,

$$f_\infty(\tilde{u}_\chi)d\tilde{u}_\chi = 4\pi \left(\frac{3}{2\pi} \right)^{3/2} \frac{\tilde{u}_\chi^2}{v_d^2} \exp\left(-\frac{3\tilde{u}_\chi^2}{2v_d^3}\right) d\tilde{u}_\chi, \quad (1.1)$$

where \tilde{u}_χ is the DM velocity in the halo, and v_d is the DM halo velocity dispersion.

Taking into account the motion of the star through the halo and the thermal motion of the constituents, which are assumed to follow a Maxwell-Boltzmann distribution, gives the relative velocity between the DM and targets, u_χ . The distribution function for the relative velocity can be expressed as [7]

$$f_{\text{MB}}(u_\chi, T_\star)du_\chi = \frac{u_\chi}{v_\star} \sqrt{\frac{3}{2\pi(v_d^2 + 3T_\star/m_i)}} \left(e^{-\frac{3(u_\chi - v_\star)^2}{2(v_d^2 + 3T_\star/m_i)}} - e^{-\frac{3(u_\chi + v_\star)^2}{2(v_d^2 + 3T_\star/m_i)}} \right) du_\chi, \quad (1.2)$$

where v_\star is the star's velocity in the halo rest frame¹, T_\star is the temperature of the star, and m_i is the mass of the target.

Returning to the large spherical shell of radius R , given the velocity distribution function, we can obtain the flux of DM through this surface. The rate of DM particles passing through a surface element $d\tilde{A}$ with velocity between u_χ and $u_\chi + du_\chi$, with an angle to the normal of $d\tilde{A}$ between $\tilde{\theta}$ and $\tilde{\theta} + d\tilde{\theta}$ and an azimuthal angle between $\tilde{\phi}$ and $\tilde{\phi} + d\tilde{\phi}$ is given by [8]

$$\frac{dN_\chi}{dt} = \frac{\rho_\chi}{m_\chi} f_{\text{MB}}(u_\chi, T_\star) \vec{u} \cdot d\tilde{\vec{A}} du_\chi \frac{d\tilde{\Omega}}{4\pi} \quad (1.3)$$

$$= \frac{\rho_\chi}{m_\chi} f_{\text{MB}}(u_\chi, T_\star) u_\chi \cos \tilde{\theta} d\tilde{A} du_\chi \frac{d\cos \tilde{\theta} d\tilde{\phi}}{4\pi} \quad (1.4)$$

$$= \frac{1}{4} \frac{\rho_\chi}{m_\chi} f_{\text{MB}}(u_\chi, T_\star) u_\chi d\tilde{A} du_\chi d\cos^2 \tilde{\theta}, \quad (1.5)$$

where we have integrated over the azimuthal angle $\tilde{\phi}$ due to the isotropy of the system. The number density of the DM is included through the ρ_χ/m_χ factor. Integrating over the area of the sphere is trivial due to isotropy, leaving us with

$$\frac{dN_\chi}{dt} = \pi \frac{\rho_\chi}{m_\chi} f(u_\chi, T_\star) u_\chi du_\chi d\cos^2 \tilde{\theta}, \quad (1.6)$$

¹This is the frame where the DM has an average velocity of zero.

with the integration interval for $\cos^2 \tilde{\theta}$ being $(0, 1)$.

As the DM begins to infall from this large distance R to a closer distance r , the star's gravitational field will boost the velocity by the local escape velocity $v_e(r)$ such that

$$w_\chi^2(r) = u_\chi^2 + v_e^2(r), \quad (1.7)$$

$$v_e^2(r) = \frac{2GM_\star}{R_\star} + \int_r^{R_\star} \frac{GM_\star(r')}{r'^2} dr'. \quad (1.8)$$

Due to the conservation of angular momentum, we can relate the angular momentum of the DM at the two distances R and r such that

$$J_\chi = m_\chi R u_\chi \sin \tilde{\theta} = m_\chi r w_\chi(r) \sin \theta \leq m_\chi r w_\chi(r) \equiv J_{\max}, \quad (1.9)$$

where θ is the incident angle of the DM at the closer distance r , and we have defined the maximum angular momentum J_{\max} corresponding to a linear DM trajectory.

Changing integration variables from $\cos^2 \tilde{\theta}$ to J_χ allows us to write the number of DM particles passing through the shell per unit volume as

$$\frac{dN_\chi}{dt} = 2\pi \frac{\rho_\chi}{m_\chi} \frac{f_{\text{MB}}(u_\chi, T_\star)}{u_\chi} r^2 w_\chi^2(r) \frac{J_\chi dJ_\chi}{J_{\max}^2} du_\chi. \quad (1.10)$$

The geometry of the system is shown in Fig. 1.1 for clarity.

The probability that the DM interacts with the constituents of the shell depends on the interaction rate, $\Omega(w_\chi)$, multiplied by the time spent in the shell, $dt = dr/\dot{r}$. Hence, the probability of scattering within the shell is

$$\Omega(w_\chi) \frac{dr}{\dot{r}} = 2\Omega(w_\chi) \frac{1}{w_\chi} \left(1 - \left(\frac{J_\chi}{rw_\chi} \right)^2 \right)^{-1/2} \Theta(J_{\max} - J_\chi) dr, \quad (1.11)$$

where the factor of 2 is due to the DM having two opportunities to pass through the shell, once when incoming and another after turning around². The step-function is put in to ensure the angular momentum does not exceed its maximum allowed value.

For a scattered DM to be considered captured, it must lose enough energy in the collision to become gravitationally bound. The rate at which a DM particle scatters from an initial velocity w_χ to a final velocity $v < v_e(r)$ is given by [5–7]

$$\Omega^-(w_\chi) = \int_0^{v_e} R^-(w_\chi \rightarrow v) dv, \quad (1.12)$$

$$R^-(w_\chi \rightarrow v) = \int n_T(r) \frac{d\sigma_{\chi T}}{dv} |\vec{w}_\chi - \vec{u}_T| f_T(u_T) d^3 \vec{u}_T, \quad (1.13)$$

²The radial velocity \dot{r} is a standard result in orbital mechanics and can be obtained from the central force Lagrangian.

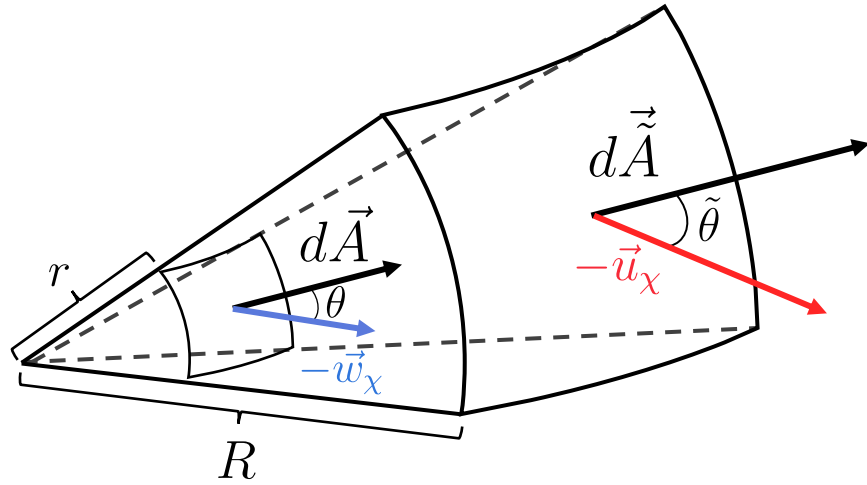


Figure 1.1: Geometry of the capture process, showing two elements of spheres with radii r close to the star

with $R^-(w_\chi \rightarrow v)$ being the differential interaction rate, n_T is the target number density, u_T is the target velocity and $f_T(u_T)$ is the corresponding distribution function, and $d\sigma_{\chi T}/dv$ is the differential cross-section. The minus superscript is used to signify that this is the down scattering rate, i.e. the rate of interactions leading to the DM losing energy.

Finally, we obtain the capture rate by multiplying Eqs. 1.10 and 1.11 and integrate over the angular momentum to give the result

$$C = \int_0^{R_*} dr 4\pi r^2 \int_0^\infty du_\chi \frac{\rho_\chi}{m_\chi} \frac{f_{\text{MB}}(u_\chi, T_*)}{u_\chi} w_\chi(r) \Omega^-(w_\chi). \quad (1.14)$$

This result is rather generic, as the choice of DM model will only dictate the form of the differential cross-section in Eq. 1.13. As written above, the distribution function for the relative velocity far from the star can be any isotropic distribution function. The MB form was chosen as it allows for a simple analytic form of the total capture rate.

1.2 Capture in Compact Objects

Having reviewed the capture process in non-relativistic stars, we can begin discussing the necessary modifications required when considering relativistic stars. In

this section, we consider the two major modifications that need to be made:

- The corrections from General Relativity due to the extreme gravitational fields. This ultimately alters the flux of DM passing through the star, boosting it through gravitational focusing.
- Accounting for the relativistic and degenerate nature of the star's constituents in the interaction rate.

The former is generic to neutron stars and white dwarfs, while the latter is required for all NS constituents, but only the electrons in a WD are degenerate and relativistic. The ions of the WD are non-relativistic and non-degenerate and, hence, can the solar capture formalism can be applied in this case.

1.2.1 General Relativistic Corrections to the Capture Rate

Far from the star, the physics is the same as in the previous section. The deviations arise as the DM falls into the gravitational potential of the star. We begin by following the DM along its trajectory, moving from a distance $R \gg R_\star$ to a closer distance r . Hence, we are working in the DM rest frame and calculating the rate at which the DM passes through the shell *per unit of proper time*, τ . The proper time interval is related to the metric through

$$d\tau^2 = B(r)dt^2 - A(r)dr^2 - r^2d\Omega^2, \quad (1.15)$$

with $B(r)$ and $A(r)$ defined in Chapter ??.

Following the same arguments as in the non-relativistic case, the flux of DM passing through the shell is

$$\frac{dN_\chi}{d\tau} = 2\pi \frac{\rho_\chi}{m_\chi} \frac{f_{\text{MB}}(u_\chi)}{u_\chi} du_\chi \frac{J_\chi dJ_\chi}{m_\chi^2}, \quad (1.16)$$

which takes the same form as Eq. 1.10, with the physical difference being that this is the rate with respect to the proper time. Additionally, as we will be considering cold stars, we take the $T_\star \rightarrow 0$ limit of the DM-target relative velocity distribution, such that

$$f_{\text{MB}}(u_\chi) = \lim_{T_\star \rightarrow 0} f_{\text{MB}}(u_\chi, T_\star) \quad (1.17)$$

$$= \frac{u_\chi}{v_\star} \sqrt{\frac{3}{2\pi(v_d^2 + 3T_\star/m_i)}} \left(e^{-\frac{3(u_\chi - v_\star)^2}{2(v_d^2 + 3T_\star/m_i)}} - e^{-\frac{3(u_\chi + v_\star)^2}{2(v_d^2 + 3T_\star/m_i)}} \right), \quad (1.18)$$

The probability that DM scatters within the shell and is captured is $2\hat{\Omega}^-(r)d\tau$, where $\hat{\Omega}^-(r)$ is the interaction rate with respect to the proper time, and $d\tau$ is the proper time taken to move from coordinate r to $r + dr$. The factor of 2 once again accounts for the DM crossing the shell twice per orbit. For calculation purposes, we need to relate this to the interaction rate seen by a distant observer, $\Omega^-(r)$, that is done through

$$\hat{\Omega}^-(r)d\tau = \frac{1}{\sqrt{g_{tt}}}\Omega^-(r)d\tau = \frac{1}{\sqrt{B(r)}}\Omega^-(r)d\tau. \quad (1.19)$$

Now, the proper time that the DM spends inside a shell of thickness dr will be³

$$d\tau = \left(\frac{d\tau}{dt}\right)dt = B(r)\frac{dr}{\dot{r}} = \frac{\sqrt{B(r)}dr}{\sqrt{\frac{1}{A(r)}\left[1 - B(r)\left(1 + \frac{J_\chi^2}{m_\chi^2 r^2}\right)\right]}}. \quad (1.20)$$

The differential capture rate can then be written as

$$dC = 2\pi \frac{\rho_\chi}{m_\chi} \frac{f_{\text{MB}}(u_\chi)}{u_\chi} du_\chi \frac{dJ_\chi^2}{m_\chi^2} \frac{\Omega^-(r)\sqrt{A(r)}dr}{\sqrt{1 - B(r)\left(1 + \frac{J_\chi^2}{m_\chi^2 r^2}\right)}}. \quad (1.21)$$

As the total number of targets in the star, N_T , needs to satisfy

$$N_T = \int_0^{R_*} 4\pi r^2 n_T(r) \sqrt{A(r)} dr, \quad (1.22)$$

where $n_T(r)$ is the number density that appears in the interaction rate, we absorb the factor $\sqrt{A(r)}$ into the definition of $n_T(r)$, such that $\Omega^-(r)\sqrt{A(r)} \rightarrow \Omega^-(r)$. This is due to the number densities obtained by solving the TOV equations already account for the $\sqrt{A(r)}$ factor.

As before, we have $w_\chi^2(r) = u_\chi^2 + v_e^2(r)$, however as the escape velocity will be significantly larger than the ambient DM velocity far from the star, we can safely approximate $w_\chi^2(r) \approx v_e^2(r)$. In the relativistic case, the escape velocity can be defined as

$$v_e^2(r) = \left(\frac{dl}{d\tau}\right)^2 = A(r) \left(\frac{dr}{d\tau}\right)^2 + r^2 \left(\frac{d\phi}{d\tau}\right)^2 = 1 - B(r), \quad (1.23)$$

where dl is a length element. The large boost from the escape velocity also removes the u_χ dependence in the kinematics of the interactions and allows us to perform the integration over the initial DM velocity, yielding an overall factor of

$$\int_0^\infty \frac{f_{\text{MB}}(u_\chi)}{u_\chi} du_\chi = \frac{1}{v_*} \text{Erf}\left(\sqrt{\frac{3}{2}} \frac{v_*}{v_d}\right). \quad (1.24)$$

³See Appendix ?? for the derivation of $\dot{r} = \frac{dr}{dt}$.

To integrate over J_χ^2 , we need the maximum angular momentum the DM can achieve as it passes through the shell. This can be obtained by requiring the argument of the radical above to remain positive, giving

$$J_{\max} = \sqrt{\frac{1 - B(r)}{B(r)}} m_\chi r. \quad (1.25)$$

The factor of $1/\sqrt{B}$ arises due to the gravitational focusing of the incoming flux of DM [9].

Putting everything together, and integrating over the radius of the star, we are left with the final result for the capture rate of

$$C = \frac{4\pi}{v_\star} \frac{\rho_\chi}{m_\chi} \text{Erf} \left(\sqrt{\frac{3}{2}} \frac{v_\star}{v_d} \right) \int_0^{R_\star} r^2 \frac{\sqrt{1 - B(r)}}{B(r)} \Omega^-(r) dr. \quad (1.26)$$

All that remains is determining the form of the interaction rates for relativistic energies.

1.2.2 Geometric Limit and Threshold Cross-Section

In the previous section, we derived an expression for the capture rate assuming that the DM is captured after a single scatter, and that it only scatters once along its orbit through the NS. This first assumption is true for DM light enough to lose enough energy in this single interaction, which for nucleon targets turns out to be $m_\chi \lesssim 10^6$ GeV. The latter assumption is a statement that we are working in the optically thin regime, such that the cross-section is much less than the “threshold cross-section”, σ_{th} . The value of the threshold cross-section is defined as the cross-section for which the capture rate evaluated in the optically thin regime is equal to the geometric limit [10],

$$C_{\text{geom}} = \frac{\pi R_\star^2 (1 - B(R_\star))}{v_\star B(R_\star)} \frac{\rho_\chi}{m_\chi} \text{Erf} \left(\sqrt{\frac{3}{2}} \frac{v_\star}{v_d} \right). \quad (1.27)$$

This is the capture rate for which the entire flux of DM passing through the surface of the star is captured at the surface. Hence, it serves as an upper bound to the capture rate, with cross-sections greater than σ_{th} saturating the capture rate to this value. Note the $1/B(R_\star)$ factor in the equation above. In stars and planets where classical Newtonian mechanics can be applied, gravitational focusing would result in a factor $v_{\text{esc}}^2/v_\star = (1 - B(R_\star))/v_\star$ in Eq. 1.27, where we have used Eqs. 1.23 and ???. In neutron stars, on the other hand, general relativity introduces an additional

factor of $1/B(R_*)$, which can be obtained from the derivation of the flux of DM particles accreted to a NS with a Schwarzschild metric (Eq. 1.26) [9, 11].

For scattering on neutrons, the threshold cross-section is approximately

$$\sigma_{th} = \begin{cases} \sigma_{ref} \frac{\text{GeV}}{m_\chi}, & m_\chi \lesssim 1 \text{ GeV} \quad (\text{Pauli blocking regime}), \\ \sigma_{ref}, & 1 \text{ GeV} \lesssim m_\chi \lesssim 10^6 \text{ GeV}, \\ \sigma_{ref} \frac{m_\chi}{10^6 \text{ GeV}}, & m_\chi \gtrsim 10^6 \text{ GeV} \quad (\text{Multiscattering regime}), \end{cases} \quad (1.28)$$

where we take the canonical value of

$$\sigma_{ref} \sim 1.7 \times 10^{-45} \text{ cm}^2, \quad (1.29)$$

which assumes the NS is a solid sphere such that $\sigma_{ref} \sim m_n \pi R_*^2 / M_*$ with m_n the neutron mass.

For scattering off other targets, Pauli blocking is relevant for $q_0^{\text{MAX}} \lesssim \mu_{\text{target}}$ while multi-scattering is relevant for $m_\chi \gtrsim q_0^{\text{MAX}} / v_*^2$, where q_0^{MAX} is the maximum energy transferred in a collision, as will be discussed later. In addition, because the other target species have a lower abundance than neutrons, the reference cross-section, σ_{ref} , will be higher. The values of σ_{th} in Eq. 1.28, and their regions of applicability, can thus be altered appropriately for other target species of interest.

1.2.3 Interaction Rate for Relativistic Energies and Degenerate Targets

Our next goal is to write down an interaction rate suitable for describing the interactions between relativistic particles and account for the degeneracy of the target species. This will be achieved by modifying the non-relativistic interaction rate of Eq. 1.12 through the use of relativistic kinematics and the use of Lorentz invariant quantities, and the correct distribution functions for degenerate fermion targets.

As shown in Eqs. 1.12 and 1.13, the interaction rate between non-relativistic, non-degenerate species i can be expressed as

$$\Omega^-(r) = \int dv \frac{d\sigma}{dv} |\vec{w}_\chi - \vec{u}_i| n_i(r) f_{\text{MB}}(u_i) d^3 u_i. \quad (1.30)$$

First, we address the degeneracy of the targets by exchanging the Maxwell-Boltzmann distribution function for a Fermi-Dirac (FD) distribution, $f_{\text{FD}}(E_i, r)$, via the replacement

$$n_i(r) f_{\text{MB}}(u_i) d^3 u_i \rightarrow \frac{g_s}{(2\pi)^3} f_{\text{FD}}(E_i, r), \quad (1.31)$$

where $g_s = 2$ is the number of spin states of the target species, p is the 3-momentum of the incoming target, and E_i is its corresponding energy. The radial dependence of the FD distribution stems from its implicit dependence on the chemical potential of the target. Rewriting this expression in a more computationally friendly manner in terms of the relevant kinematic quantities results in

$$\frac{g_s}{(2\pi)^3} f_{\text{FD}}(E_i, r) = \frac{p E_i}{2\pi^2} f_{\text{FD}}(E_i, r) dE_i d\cos\theta_{uw}, \quad (1.32)$$

where we have expressed the angular component of the d^3p differential in terms of the angle between the incoming DM and target. This angle can be traded for the more useful quantity s , the centre of mass energy through

$$\frac{d\cos\theta_{uw}}{ds} = \frac{1}{2pp_\chi} = \frac{1}{2p\sqrt{E_\chi^2 - m_\chi^2}} = \frac{1}{2pm_\chi} \sqrt{\frac{B(r)}{1 - B(r)}}, \quad (1.33)$$

as the initial DM energy is $E_\chi = m_\chi/\sqrt{B(r)}$.

Next, we calculate the initial relative velocity, $|\vec{w}_\chi - \vec{u}_i|$, using relativistic kinematics, expressing it in terms of the Mandelstam s ,

$$|\vec{w}_\chi - \vec{u}_i| = \frac{\sqrt{s^2 - 2s(1 + \mu^2)m_i^2 + (1 - \mu^2)^2m_i^4}}{s - (1 + \mu^2)m_i^2}, \quad (1.34)$$

where $\mu = m_\chi/m_i$.

Given that it is most common to present the relativistic differential scattering cross-section $d\sigma/d\cos\theta_{\text{cm}}$ as a function of the Mandelstam variables s and t , with θ_{cm} the centre of mass frame scattering angle, we make the replacement

$$dv \frac{d\sigma}{dv} = dt \frac{d\sigma}{dt} = dt \frac{d\sigma}{d\cos\theta_{\text{cm}}} \frac{d\cos\theta_{\text{cm}}}{t}. \quad (1.35)$$

The final Jacobian factor can be expressed as

$$\frac{d\cos\theta_{\text{cm}}}{dt} = \frac{2s}{s^2 - 2s(1 + \mu^2)m_i^2 + (1 - \mu^2)^2m_i^4}, \quad (1.36)$$

for the elastic scattering we consider here.

Finally, we note that the first application of this capture formalism was for neutron targets, with the analysis completed before we had considered the additional effects from the form factors and strong interactions discussed in subsection ???. These effects will be incorporated into this formalism in a self-consistent way next chapter. The initial approach that was taken to account for the fact that we are

using realistic neutron number density profiles, despite the expression in Eq. 1.31 being for a free Fermi gas, is to introduce a correction factor as in Ref. [12],

$$\zeta(r) = \frac{n_i(r)}{n_{\text{free}}(r)}, \quad (1.37)$$

where $n_{\text{free}}(r)$ is obtained by integrating Eq. 1.32 over all phase space. In the zero-temperature approximation, the result is

$$n_{\text{free}}(r) = \frac{1}{3\pi^2} [\varepsilon_{F,i}(r)(2m_i + \varepsilon_{F,i}(r))]^{3/2}. \quad (1.38)$$

Compiling everything together leads to the final expression for the interaction rate being

$$\Omega^-(r) = \int dt dE_i ds \zeta(r) \frac{d\sigma}{d \cos \theta_{\text{cm}}} \frac{E_i}{2\pi^2 m_i} \sqrt{\frac{B(r)}{1 - B(r)}} \frac{s}{\beta(s)\gamma(s)} \times f_{\text{FD}}(E_i, r)(1 - f_{\text{FD}}(E'_i, r)), \quad (1.39)$$

where we have introduced the helper functions

$$\beta(s) = s - (m_i^2 + m_\chi^2), \quad (1.40)$$

$$\gamma(s) = \sqrt{\beta^2(s) - 4m_i^2 m_\chi^2}. \quad (1.41)$$

We have also introduced the Pauli blocking factor, $1 - f_{\text{FD}}(E'_i, r)$, to account for the phase space available to the final state target. The energy of this final state particle, E'_i , is in general a messy function of E_i , t , s , and r , and can be obtained from the kinematics of the scattering. This result is presented in Appendix ??.

The integration intervals are

$$t_{\min} = -\frac{\gamma(s)}{s}, \quad (1.42)$$

$$t_{\max} = 0, \quad (1.43)$$

$$s_{\min} = m_i^2 + m_\chi^2 + 2\frac{E_i m_\chi}{\sqrt{B(r)}} - 2m_\chi \sqrt{\frac{1 - B(r)}{B(r)}} \sqrt{E_i^2 - m_i^2}, \quad (1.44)$$

$$s_{\max} = m_i^2 + m_\chi^2 + 2\frac{E_i m_\chi}{\sqrt{B(r)}} + 2m_\chi \sqrt{\frac{1 - B(r)}{B(r)}} \sqrt{E_i^2 - m_i^2}, \quad (1.45)$$

$$E_{i,\min} = m_i, \quad (1.46)$$

$$E_{i,\max} = \frac{m_i}{\sqrt{B(r)}}. \quad (1.47)$$

As we will be dealing with NSs at low temperatures, we can take the $T_\star \rightarrow 0$ limit and replace the FD functions with step functions,

$$f_{\text{FD}}(E_i, r) \rightarrow \Theta(\varepsilon_{F,i}(r) + m_i - E_i), \quad (1.48)$$

$$1 - f_{\text{FD}}(E'_i, r) \rightarrow \Theta(E'_i - m_i - \varepsilon_{F,i}(r)). \quad (1.49)$$

The first step function can be used to further restrict the E_i integration interval to be $[m_i, m_i + \varepsilon_{F,i}(r)]$. In practice, we work with the kinetic energies of the targets rather than their total energy, as this is the quantity that directly changed in the interactions. Therefore, unless otherwise specified, we will take E_i to mean the target kinetic energy, with the integration range being $0 \leq E_i \leq \varepsilon_{F,i}$.

This expression resembles that of Ref. [12], but uses a relativistic formalism instead. In Appendix ??, we show that Eq. 1.39 reduces to the classical expression for the interaction rate in the non-relativistic limit.

1.3 The Differential Interaction Rate

In the previous section, we have calculated the interaction rate, $\Omega^-(r)$, assuming the initial DM energy takes its pre-capture value, $E_\chi = m_\chi/B(r)$. However, we are also interested in an expression for the interaction rate valid for arbitrary DM energy. This will be required when we consider capture via multiple scatterings, and it will also be necessary to study the subsequent scattering interactions that follow capture and lead to the DM thermalising within the NS. In principle, it is possible to calculate this rate numerically by binning Ω^- , Eq. 1.39, in the energy loss, i.e. multiplying Ω^- by $\frac{1}{E_i - E_j} \Theta(E_i + E_i - E'_i) \Theta(E'_i - E_i - E_j)$ and integrating over the bin $[E_j, E_i]$. However, it is possible to derive analytic expressions for the differential rate, valid in the zero-temperature approximation. To do so, we use the definition of the scattering rate in Ref. [13, 14]

$$\begin{aligned} \Gamma^-(E_\chi) = 2 \int \frac{d^3 k'}{(2\pi)^3} \int \frac{d^3 p}{(2\pi)^3} \int \frac{d^3 p'}{(2\pi)^3} \frac{|\bar{\mathcal{M}}|^2}{(2E_\chi)(2E'_\chi)(2E_i)(2E'_i)} \\ \times (2\pi)^4 \delta^4(k_\mu + p_\mu - k'_\mu - p'_\mu) f_{\text{FD}}(E_i)(1 - f_{\text{FD}}(E'_i)), \end{aligned} \quad (1.50)$$

where $|\bar{\mathcal{M}}|^2$ is the squared matrix element, $k^\mu = (E_\chi, \vec{k})$ and $k'^\mu = (E'_\chi, \vec{k}')$ are the DM initial and final momenta, and $p^\mu = (E_i, \vec{p})$ and $p'^\mu = (E'_i, \vec{p}')$ are the target particle initial and final momenta, respectively. To see that Γ^- is indeed the same as Ω^- in Eq. 1.39, multiply and divide by $v_{\text{rel}} = |\vec{w} - \vec{u}_i|$ to reintroduce the quantum

field theoretic definition of differential cross-section,

$$d\sigma = \frac{|\mathcal{M}|^2}{2E_\chi 2E_i |\vec{w} - \vec{w}_i|} d^2\Pi_{\text{LIPS}}, \quad (1.51)$$

$$d^2\Pi_{\text{LIPS}} = \frac{1}{2E'_\chi} \frac{d^3k'}{(2\pi)^3} \frac{1}{2E'_i} \frac{d^3p'}{(2\pi)^3} (2\pi)^4 \delta^4(k_\mu + p_\mu - k'_\mu - p'_\mu), \quad (1.52)$$

$$\implies \frac{d\sigma}{d\cos\theta_{\text{cm}}} = \frac{1}{16\pi} \frac{\beta(s)}{2s\beta(s) - \gamma^2(s)} |\mathcal{M}|^2, \quad (1.53)$$

where $d^2\Pi_{\text{LIPS}}$ is the 2-body Lorentz invariant phase space.

The advantage of Eq. 1.39 is that it can be used to calculate the capture rate for any interaction given the differential cross-section. The disadvantage is that this computation has to be evaluated numerically, which can be computationally intensive. For this reason, shall now use Eq. 1.50 to derive analytic expressions that will allow us to speed up computations and, in addition, calculate the shape of the interaction rate as a function of the energy loss.

The interaction rate for $d\sigma \propto s^m t^n$ is

$$\begin{aligned} \Gamma^-(E_\chi) = & \sum_{n,m} \frac{(-1)^n \alpha_{n,m}}{128\pi^3 E_\chi k} \int_0^{E_\chi - m_\chi} dq_0 \int \frac{dt_E t_E^n}{(t_E + q_0^2)^{m+\frac{1}{2}}} \\ & \times \sum_{r=0}^m \mathcal{V}_{m,r} \sum_{j=0}^r \binom{r}{j} \varepsilon_{F,i}^{r-j} \frac{(-1)^j q_0^{j+1}}{j+1} h_j \left(\frac{E_i^{t^-} - \varepsilon_{F,i}}{q_0} \right), \end{aligned} \quad (1.54)$$

for elastic scattering with $t_E = -t = q^2 - q_0^2$, where $q_0 = E'_i - E_i$ is the DM energy loss,

$$E_i^{t^-} = - \left(m_n + \frac{q_0}{2} \right) + \sqrt{\left(m_n + \frac{q_0}{2} \right)^2 + \left(\frac{\sqrt{q^2 - q_0^2}}{2} - \frac{m_n q_0}{\sqrt{q^2 - q_0^2}} \right)^2}, \quad (1.55)$$

is the minimum energy of the neutron before the collision, obtained from kinematics, and $h_j(x)$ is a step function with a smooth transition,

$$h_j(x) = \begin{cases} 0, & x > 0 \\ (-x)^{j+1}, & -1 < x < 0 \\ 1, & x < -1 \end{cases} \quad (1.56)$$

The full derivation of this interaction rate can be found in Appendix A. Our result for Γ^- is an extension of that presented in Ref. [14], where the interaction rate was calculated only in the case of low energy and a constant matrix element. It

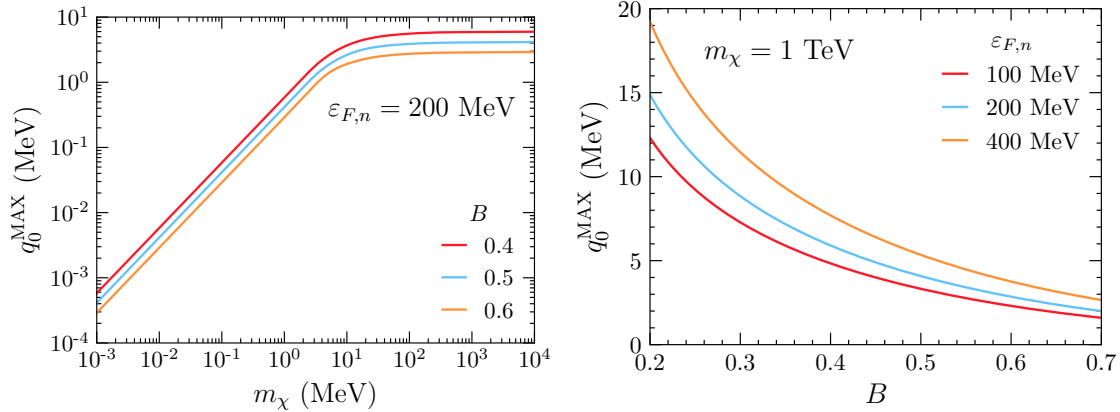


Figure 1.2: Left: q_0^{MAX} vs. m_χ for $\epsilon_{F,n} = 200 \text{ MeV}$ and different values of B . Right: q_0^{MAX} as a function of B for different values of $\epsilon_{F,i}$ and $m_\chi = 1 \text{ TeV}$.

is valid at all energy ranges. The differential interaction rate $\frac{d\Gamma}{dq_0}(E_\chi, q_0)$ is then just the integrand of Eq. 1.54. We will use $\frac{d\Gamma}{dq_0}$ to obtain normalised shapes for the differential interaction spectrum, while we will use Ω^- when we need the total interaction rate, such as in the capture rate.

Kinematics, and the phase space allowed by $h_j(x)$ in Eq. 1.54, determine the maximum energy that a DM particle can lose in a single scattering interaction, q_0^{MAX} . The details of how to obtain q_0^{MAX} are given in Appendix A.2.1. For DM capture, the value of q_0^{MAX} depends primarily on the DM mass, as is illustrated in the left panel of Fig. 1.2. We can see that for low m_χ , $q_0^{\text{MAX}} \propto m_\chi$, while, for $m_\chi \gg m_n$, it plateaus to values between $q_0^{\text{MAX}} \sim 3 - 6 \text{ GeV}$. Both q_0^{MAX} and $\frac{d\Gamma}{dq_0}$ also depend on $\epsilon_{F,n}$ and B . Changing $\epsilon_{F,n}$ has a very mild effect on the value of q_0^{MAX} (see right panel of Fig. 1.2) and on the shape of the normalised spectrum (see Fig. 1.3). On the other hand, increasing B has the main effect of reducing q_0^{MAX} (see right panel of Fig. 1.2), but only a mild effect on the shape of the profile expressed as a function of the normalised energy loss

$$q_0^{\text{norm}} = \frac{q_0}{q_0^{\text{MAX}}}. \quad (1.57)$$

We apply our results for $\frac{d\Gamma}{dq_0}$ to DM-neutron interactions, and in particular those with differential cross-sections that depend only on the transferred momentum $t = (k^\mu - k'^\mu)^2$ and not on the centre of mass energy $s = (p^\mu + k^\mu)^2$.

In Fig. 1.3 we show the normalised differential rates as a function of q_0^{norm} for the four operators D1-D4. The left-hand panels are in the limit $m_\chi \gg m_n$. We can observe that D1 has a softer spectrum, while the D2 and D4 spectra peak towards higher values of q_0 . Varying the chemical potential $\epsilon_{F,n}$ has a very mild effect, shifting the spectrum to lower values of q_0 with increasing values of $\epsilon_{F,n}$.

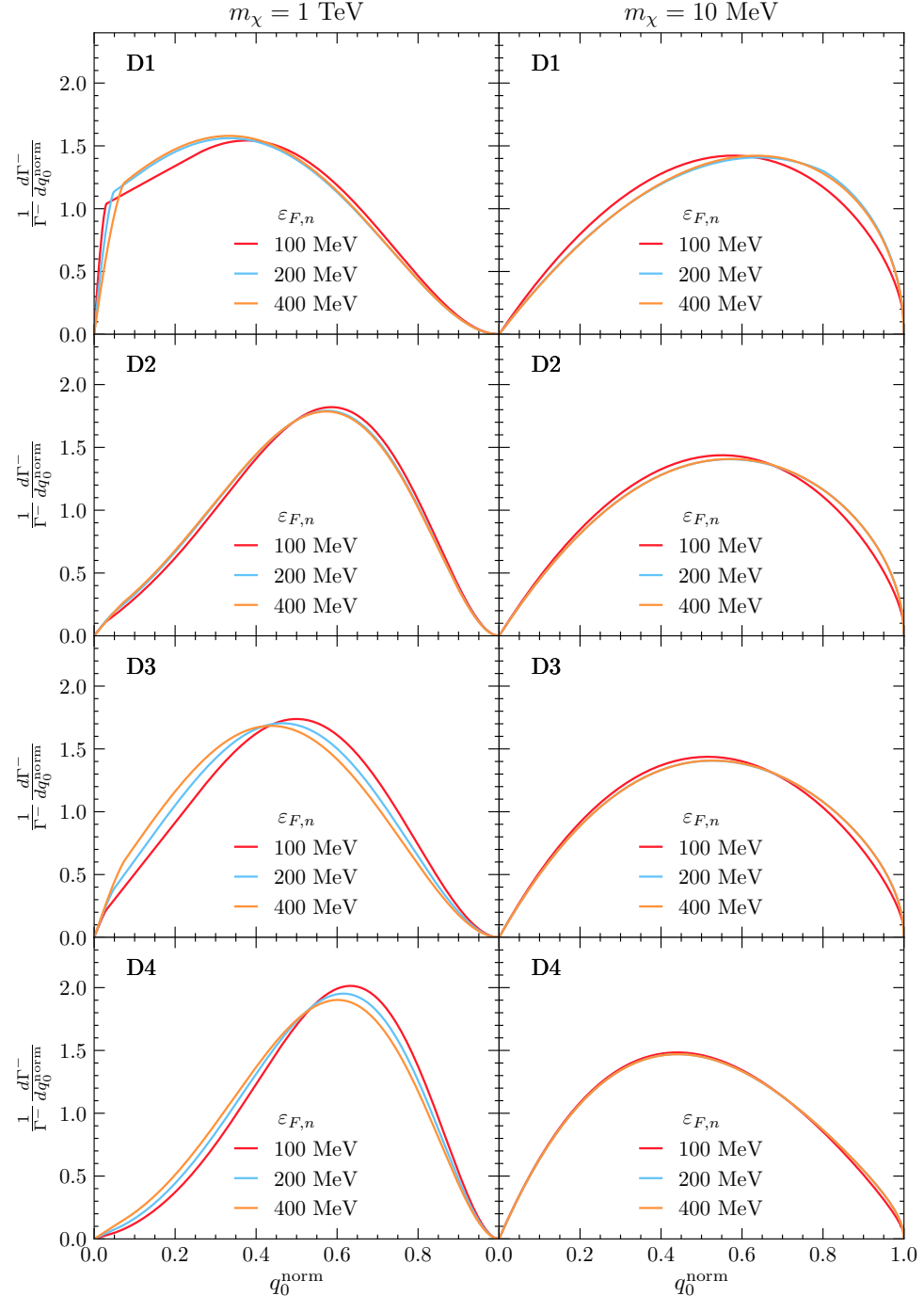


Figure 1.3: Normalised differential interaction rates $\frac{1}{\Gamma} \frac{d\Gamma}{dq_0^{\text{norm}}}$ as a function of q_0^{norm} for different values of $\varepsilon_{F,n}$, $m_\chi = 1 \text{ TeV}$ (left) and $m_\chi = 10 \text{ MeV}$ (right), $B = 0.5$ and operators D1 (first row), D2 (second row), D3 (third row) and D4 (fourth row). Profiles do not depend on m_χ in the limits $m_\chi \gg m_n$ (left) and $m_\chi \ll m_n$ (right).

Note that at small values of q_0^{norm} there is a sudden change in the slope of the normalised differential rate, which occurs for all operators but is more evident in D1 (top left panel). This is due to the zero temperature approximation, implicit in Eq. 1.54, where Heaviside functions were used to approximate FD distributions (see Appendix A.2.1); using a finite temperature would produce a smoother spectrum at small q_0^{norm} .

In the right-hand panels of Fig. 1.3, we explore the low DM mass region $m_\chi \ll m_n$. In this case, all operators give rise to similar profiles, the sole difference being that the peak of the profile is now shifted to lower q_0^{norm} for D4 in contrast to D1, with intermediate values for D2 and D3. This is a consequence of Pauli blocking, with this effect depending on the specific power of t that dominates the spectrum. Profiles with lower n ($d\sigma \propto t^n$) peak at higher q_0^{norm} (see Fig. 1.3, right panels). For D4 we have $|\bar{\mathcal{M}}|^2 \propto t^2$, while the matrix elements of D2 and D3 are linear combinations of t and t^2 , and D1 is a combination of all powers of t . Comparing the right panels of Fig. 1.3 with Fig. A.2, we observe that the lowest power of t determines the shape of the final differential interaction rate. Finally, varying $\varepsilon_{F,n}$ has a very mild effect, this time shifting the spectrum mostly to higher values of q_0 for higher $\varepsilon_{F,n}$.

The fact that the lowest power of t dictates the features of the differential interaction rate is true also for the interactions that have a dependence on s . As such, by understanding the properties of the interaction rates with $|\bar{\mathcal{M}}|^2 \propto t^n$, we can understand the rates for all the operators in Table ??.

1.3.1 Pauli Blocking

The DM interaction rate, Eq. 1.50, will be proportional to the number of target particles available to scatter off. Classically, this is the total number of targets within the star. However, the quantum degeneracy of the species within compact objects, due to the extreme densities, leads to a reduction in the number of available initial state target particles the DM can scatter off. To understand this, consider the $T \rightarrow 0$ approximation, in which all initial states with energies $E_i < \varepsilon_{F,i}$ are occupied. These states are known as the “Fermi sea”. In order for the DM to scatter off one of these states, it must impart enough energy to kick the target out of the Fermi sea, such that

$$E'_i = E_i + q_0 > \varepsilon_{F,i}, \quad (1.58)$$

imposing a lower limit on the energy transfer required for an interaction to take place. This effectively reduces the number of available targets to only those with kinetic energies between $\varepsilon_{F,n} - q_0$ and $\varepsilon_{F,i}$. This suppression of the initial state phase space is known as Pauli blocking (PB), and is a completely quantum phenomenon.

In this limit, we necessarily have $\Gamma^- \rightarrow 0$ for $q_0 \rightarrow 0$. It is also worth noting that Pauli blocking only affects the interaction rate when $q_0 \leq \varepsilon_{F,n}$.

To assess the impact of PB on the DM differential interaction rate, in Fig. 1.4 we compare the rate with (blue solid lines) and without (light blue dashed lines) Pauli blocking, for $B = 0.5$ and constant DM-neutron cross-section. When Pauli blocking can be neglected, the interaction rate is obtained straightforwardly from Eq. 1.50 by stripping away the $(1 - f_{FD}(E'_i))$ factor. The difference between the computations is shaded in light blue. In the top left panel, we see that the rate begins to be suppressed from PB at $q_0 \sim \varepsilon_{F,i} = 100$ MeV for a 1 GeV DM. In the top right plot, we increase the neutron chemical potential from $\varepsilon_{F,n} = 100$ MeV to $\varepsilon_{F,n} = 400$ MeV. Given that in this case $q_0^{\text{MAX}} \sim 0.4m_\chi \sim 400$ MeV, almost the whole energy range is affected by PB. The higher $\varepsilon_{F,n}$ changes the spectra (both with and without PB) such that the unsuppressed rate is no longer flat at low q_0 . The PB suppressed rate reaches a maximum at values of q_0 slightly below q_0^{MAX} , and then decreases towards 0 at lower q_0 . In the middle panels, $m_\chi = 100$ MeV, and $q_0^{\text{MAX}} \sim 40$ MeV $\ll \varepsilon_{F,n}$. In this case, it is evident that PB affects the spectrum over the full $q_0 = q_0^{\text{MAX}}$ range. In the bottom row, we set $m_\chi = 10$ MeV. As expected, for lighter DM, the effects of PB are even more pronounced.

To understand how the effect of PB varies throughout the star, we can analyse the radial profiles of the capture rates dC/dr . In Fig. 1.5 we plot the differential capture rate as a function of the NS radius, with and without Pauli blocking. We see that Pauli blocking is most significant at low DM mass, below about 1 GeV, and becomes insignificant for higher masses. Pauli blocking has a larger impact on the differential capture rate deeper into the NS interior and has a negligible effect at the surface. This is particularly apparent in the top left panel of Fig. 1.5. This is because the chemical potential is higher in the NS interior than it is near the crust, as seen in the radial $\varepsilon_{F,i}$ profile in the bottom left panel of Fig. ??.

1.4 Capture in the Low, Intermediate and High Mass Regimes

Having assembled all the required machinery, we are ready to explore the properties of the capture rate in the three mass regimes outlined in Eq. 1.28. Given the computational load required to evaluate Eq. 1.26 in general, we aim to provide approximations that are numerically more efficient where possible. We also discuss the high DM mass regime where multiple scatterings are required for capture, and how this is affected by Pauli blocking.

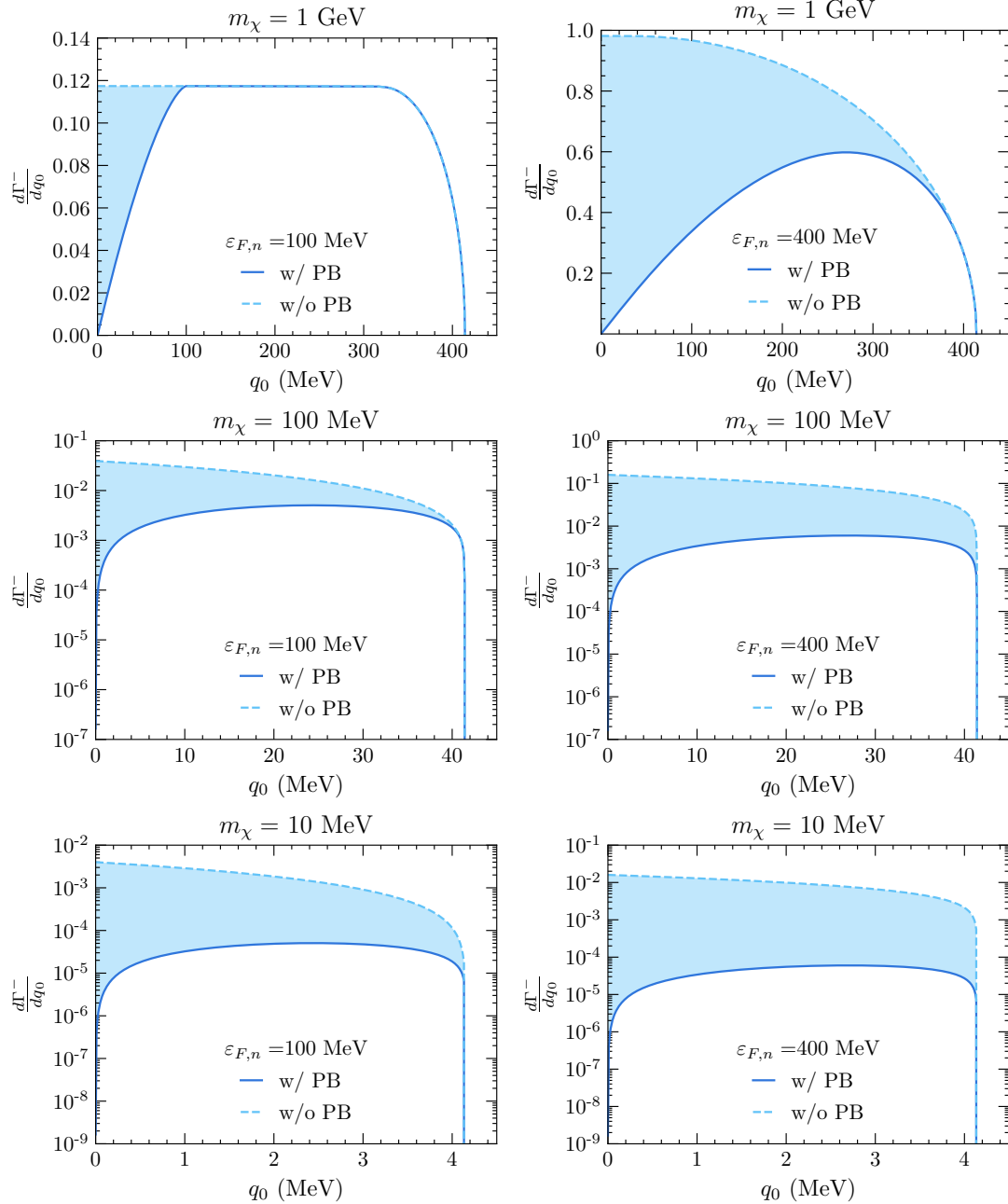


Figure 1.4: Differential interaction rates $d\Gamma/dq_0$ as a function of the energy loss q_0 for different values of m_χ and $\varepsilon_{F,n}$, constant cross-section and $B = 0.5$. Blue lines refer to the result that includes Pauli blocking, while the light blue dashed lines refer to the result without PB. Left column: $\varepsilon_{F,n} = 100 \text{ MeV}$, right column: $\varepsilon_{F,n} = 400 \text{ MeV}$. Top: $m_\chi = 1 \text{ GeV}$, middle: $m_\chi = 100 \text{ MeV}$, bottom: $m_\chi = 10 \text{ MeV}$.

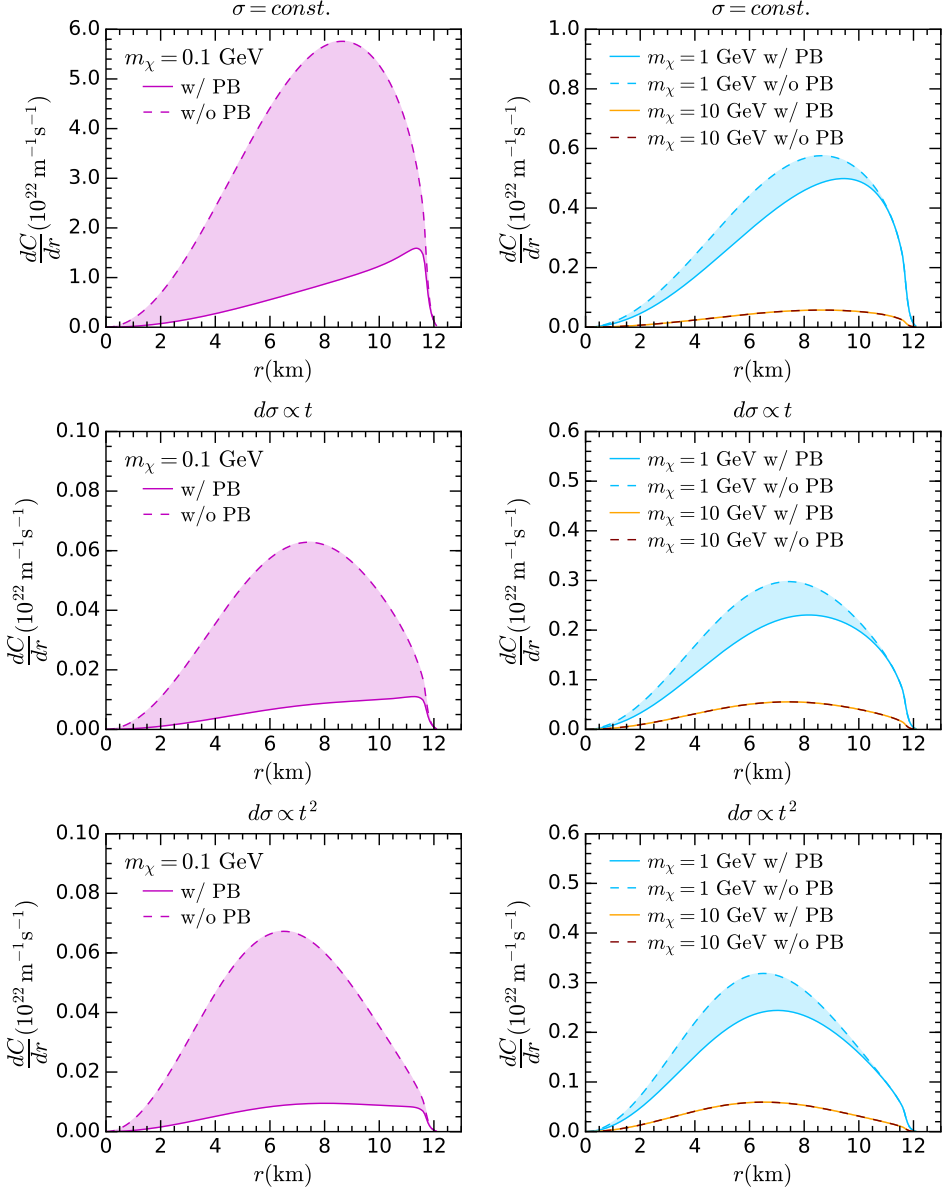


Figure 1.5: Differential capture rate as a function of the NS radius r , with (solid) and without (dashed) Pauli blocking, for the EoS benchmark BSk24-2. Top: constant cross-section, center: $d\sigma \propto t$, bottom: $d\sigma \propto t^2$.

1.4.1 Low and intermediate DM mass range

In sections 1.2 and 1.3, we have derived general expressions to numerically calculate the DM capture and interaction rates, Eqs. 1.26 and 1.39 respectively. Using these expressions, we can write the complete expression for the capture rate as a function of the differential DM-neutron cross-section

$$C = \frac{2\rho_\chi}{\pi v_\star m_\chi^2} \text{Erf} \left(\sqrt{\frac{3}{2}} \frac{v_\star}{v_d} \right) \int_0^{R_\star} dr \frac{r^2 \zeta(r)}{\sqrt{B(r)}} \int dt dE_i ds \frac{d\sigma}{d \cos \theta_{\text{cm}}} \frac{E_i s}{\beta(s) \gamma(s)} (1.59) \\ \times f_{\text{FD}}(E_i, r) (1 - f_{\text{FD}}(E'_i, r)),$$

where the functions β and γ were given in section 1.2.3. Recall that in the limit $T \rightarrow 0$, $f_{\text{FD}}(E_i, r)$ and $1 - f_{\text{FD}}(E'_i, r)$ reduce to the step functions, $\Theta(\varepsilon_{F,i}(r) - E_i)$ and $\Theta(E'_i - \varepsilon_{F,i}(r))$, respectively.

Exchanging the differential cross-section for the squared matrix allows for easier examination of the operators in Table ??, and so we write the capture rate as

$$C = \frac{\rho_\chi}{8\pi^2 v_\star m_\chi^2} \text{Erf} \left(\sqrt{\frac{3}{2}} \frac{v_\star}{v_d} \right) \int_0^{R_\star} dr \frac{r^2 \zeta(r)}{\sqrt{B(r)}} \int dt dE_i ds \frac{|\bar{\mathcal{M}}|^2 E_i}{2s\beta(s) - \gamma^2(s)} \frac{s}{\gamma(s)} (1.60) \\ \times f_{\text{FD}}(E_i, r) (1 - f_{\text{FD}}(E'_i, r)).$$

This expression can be used to numerically calculate the single scatter capture rate of DM in compact objects, in the optically thin regime. In general, this must be used for low-mass DM where PB is in effect.

As discussed in section 1.3.1, PB eventually becomes negligible for DM with masses $\gtrsim \mu_{F,i}$. Hence, between this mass and the point where multiple scattering becomes important, PB can be neglected and a simplified capture rate be obtained. For nucleon targets, this range is between $1 \text{ GeV} \lesssim m_\chi \lesssim 10^6 \text{ GeV}$, which we call the intermediate mass range.

The resulting simplified capture rate differs slightly depending on whether the matrix element depends only on t , or if it has explicit s dependence. We present the full derivations of these results in Appendix A.5 First, for $|\bar{\mathcal{M}}|^2 = at^n$, the previous expression can be simplified to

$$C \sim C_{\text{approx}} = \frac{4\pi}{v_\star} \frac{\rho_\chi}{m_\chi} \text{Erf} \left(\sqrt{\frac{3}{2}} \frac{v_\star}{v_d} \right) \int_0^{R_\star} r^2 dr n_i(r) \frac{1 - B(r)}{B(r)} \langle \sigma(r) \rangle, (1.61)$$

$$\langle \sigma(r) \rangle = \left\langle \int dt \frac{d\sigma}{dt} \right\rangle_s = \frac{a}{16\pi m_\chi^2} \frac{1}{n+1} \left(\frac{4(1 - B(r))m_\chi^2}{B(r)(1 + \mu^2)} \right)^n. (1.62)$$

For s -dependent matrix elements the result is very similar, with the only difference being that the cross-section is not averaged over s , and instead s is fixed to a

particular value as detailed in Appendix A.5. Writing the matrix element as $|\bar{\mathcal{M}}|^2 \propto \bar{g}(s)t^n$, for with g some function of s , we arrive at the result

$$C \sim C_{\text{approx},s} = \frac{4\pi}{v_\star} \frac{\rho_\chi}{m_\chi} \text{Erf} \left(\sqrt{\frac{3}{2}} \frac{v_\star}{v_d} \right) \int_0^{R_\star} r^2 dr n_i(r) \frac{1 - B(r)}{B(r)} \sigma(r), \quad (1.63)$$

$$\begin{aligned} \sigma(r) &= \int dt \frac{d\sigma}{dt} = \frac{1}{16\pi \left(m_i^2 m_\chi^2 + 2m_i m_\chi / \sqrt{B(r)} \right)} \frac{\bar{g}(s_0)}{(n+1)} \\ &\quad \times \left[\frac{4(1 - B(r))m_\chi^2}{B(r)(1 + \mu^2) + 2\sqrt{B(r)}\mu} \right]^n, \end{aligned} \quad (1.64)$$

$$s_0 = m_i^2 + m_\chi^2 + 2 \frac{E_i m_\chi}{\sqrt{B(r)}}. \quad (1.65)$$

As with the differential interaction rates, it is the t -dependence of the matrix elements that dictate the key features of the capture rate.

In Fig. 1.6, we show the capture rate as a function of the DM mass for matrix elements proportional to t^n , for $n = 0, 1, 2$ and the NS benchmark model BSk24-2. Numerical results obtained using Eq. 1.60 are shown in solid red; results using the same equation but removing the theta function that enforces Pauli blocking are depicted in light blue; and the approximation for intermediate DM masses, Eq. 1.61, in yellow. We show the geometric limit, Eq. 1.27, in blue for comparison. The capture rates were all normalised to the geometric limit at large DM mass where PB is negligible. In the same plots, we also show in brown the result obtained from using a modified version of Eq. 1.61 to include Pauli blocking. This is achieved by including the ratio between the differential the interaction rate, Γ^- , calculated with and without Pauli blocking. This comparison was done in section 1.3.1 for various values of B and $\varepsilon_{F,n}$.

From Fig. 1.6, we can see that Eq. 1.61 is indeed a good approximation to the numerical results obtained without Pauli blocking, and can be safely used for DM masses from a few GeV up to $m_\chi \sim 10^6$ GeV, where multiple scattering becomes relevant. On the other hand, for $m_\chi \lesssim 100$ MeV the brown line is no longer a good approximation to the numerical result with Pauli blocking, as it always overestimates the capture rate by nearly an order of magnitude. Therefore, to accurately account for the effects of PB for low mass DM, the complete expression for the capture rate, Eq. 1.60 must be used and evaluated numerically.

We now compare our full numerical capture rate calculation, Eq. 1.60, with that of Ref. [12], in Fig. 1.7. The capture rates calculated in Ref. [12] correctly include the stellar structure and Pauli blocking, however, they do not account for general relativistic corrections, and the authors only considered the case of a constant cross-section, $\sigma = 10^{-45} \text{ cm}^2$. To make the comparison as fair as possible, we have

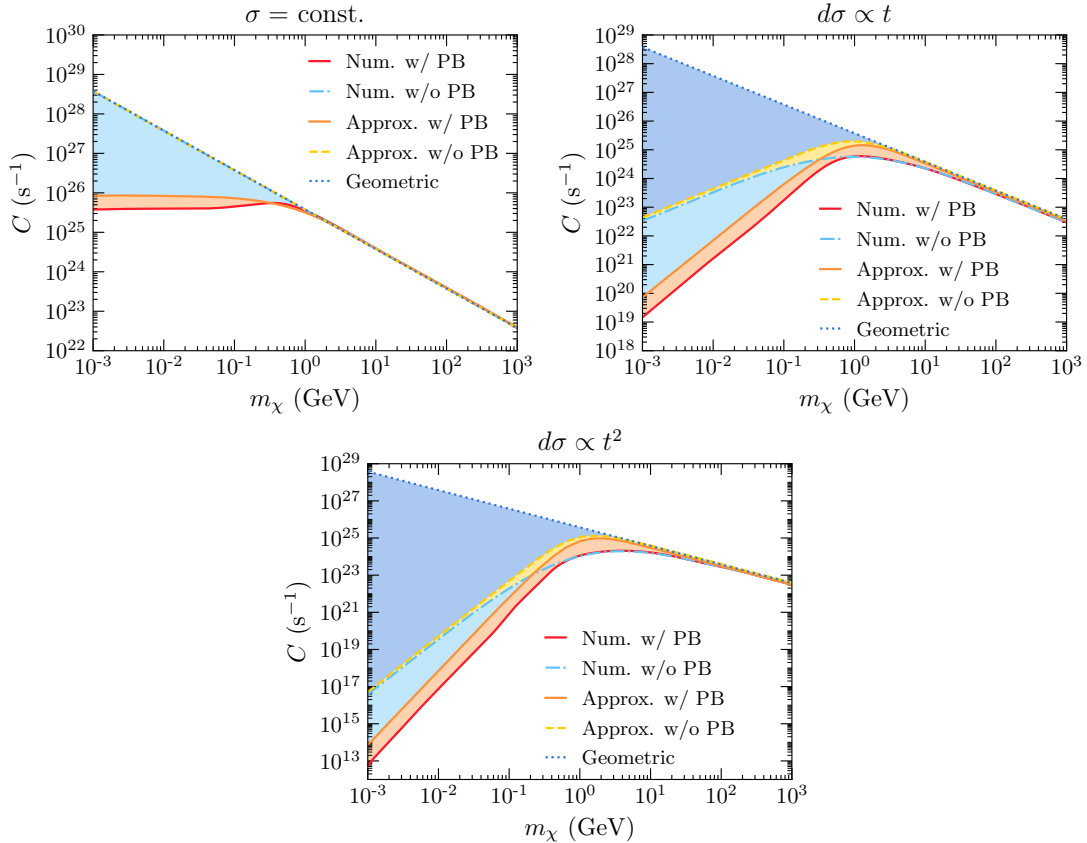


Figure 1.6: Capture rate as a function of the DM mass with cross-sections normalised to $\sigma = \sigma_{\text{ref}} \sim 1.7 \times 10^{-45} \text{ cm}^2$, for EoS BSk24-2, calculated with and without Pauli blocking. Top left: constant cross-section. Top right: $d\sigma \propto t$, bottom: $d\sigma \propto t^2$, where t is the Mandelstam variable. All rates are normalised to the geometric limit at large DM mass.

selected NS configurations that match those of Figs. 1 and 14 of Ref. [12], namely their Model A (BSk20-1): $M_\star \simeq 1.52M_\odot$, $R_\star \simeq 11.6$ km and Model D (BSk21-2): $M_\star \simeq 2.11M_\odot$ and $R_\star \simeq 12.0$ km. We denote these new benchmark models as BSk26-1 (left panel of Fig. 1.7) and BSk24-5 (right panel). Note that we were not able to use the BSk20 and BSk21 functionals, since there are no publicly available fits for the chemical potentials and particle abundances for those EoS families. However, as discussed earlier in section ??, BSk26 (BSk24) yields configurations that are almost indistinguishable from those obtained with BSk20 (BSk21) [15].

We can see in the left panel of Fig. 1.7 that in the non-Pauli suppressed region, $m_\chi \gtrsim 1$ GeV, our capture rate calculation in the optical thin limit (solid magenta) exceeds that of Ref. [12] (dot-dashed blue) by a factor of ~ 4 . When Pauli blocking is active, our capture rate calculation is about one order of magnitude higher than the classical calculation. Recall that Ref. [12] accounts for neither gravitational focusing nor relativistic kinematics. We also show in dashed light blue the approximation given in Ref. [16], which accounts for Pauli blocking with a suppression factor that depends on the neutron Fermi momentum $\sim m_\chi v_{esc}/p_{F,n}$ for $m_\chi < m_n$. Though this approximation fails to reproduce the capture rate shape due to Pauli blocking in the DM mass range [0.1 GeV, 10 GeV], it underestimates the capture rate by only a factor of 2 when the DM mass is below 0.1 GeV. Finally, we compare the geometric limit of Eq. 1.27 (solid orange) that incorporates GR effects [10] with the non-relativistic expression in Ref. [12] (dot-dashed brown). We observe that the former is $\sim 67\%$ greater than the latter, mostly due to the $1/B(R_\star)$ GR correction [9, 11]. Similar conclusions are obtained when comparing capture rate calculations for Model D of Ref. [12] (their Fig. 14) with our approach, as illustrated in the right panel of Fig. 1.7.

1.4.2 Large Mass Regime: Multiple Scattering

The capture rate expressions obtained in the previous section assume that the cross-section is small enough that the star is in the “optically thin” regime, and that a single scatter is sufficient to capture the DM. These assumptions break down if the DM-target cross-section is $\gtrsim \mathcal{O}(\sigma_{th})$, or if the DM mass exceeds $m_\chi \sim 10^6$ GeV, respectively. In this section, we focus on addressing the latter concern as we work in the optically thin regime for the remainder of this work⁴. To that end, we now explain how to modify our previous capture rate expressions to account for multiple scattering in a degenerate media⁵.

In deriving Eq. 1.59 we had assumed that the DM velocity at infinity, u_χ , can

⁴The discussion on the effect of the NS opacity in $\sigma \sim \sigma_{th}$ regime can be found in Ref. [1].

⁵For a recent discussion on multiple scattering within non-relativistic stars, or with ions in WDs, see Ref. [18].

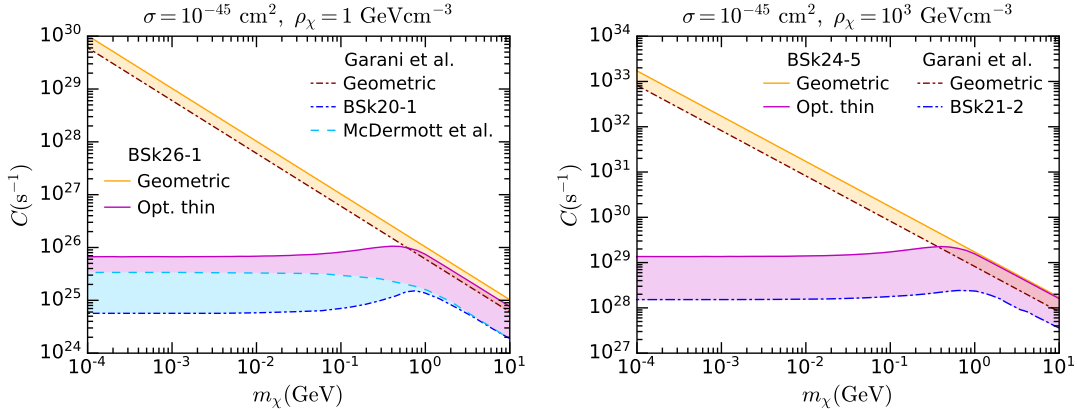


Figure 1.7: Left: Capture rate in the optically thin (magenta) and geometric (orange) limits as a function of the DM mass for constant cross-section $\sigma = 10^{-45} \text{ cm}^2$, $\rho_\chi = 1 \text{ GeV cm}^{-3}$ and BSk26 functional for $M_\star \simeq 1.52M_\odot$ and $R_\star \simeq 11.6 \text{ km}$ denoted as BSk26-1. Capture rate calculations from Ref. [12] for a NS configuration with EoS BSk20-1 [17] equivalent to BSk26-1, are shown for comparison. Right: Same as left but for $\rho_\chi = 10^3 \text{ GeV cm}^{-3}$ and the benchmark model BSk24-5 equivalent to BSk21-2 in Ref. [12]: $M_\star \simeq 2.11M_\odot$ and $R_\star \simeq 12.0 \text{ km}$.

be neglected, such that any interaction where the DM loses energy resulted in its capture. If we instead keep the leading order u_χ contribution to the total DM energy, the DM energy at infinity is

$$E_\chi^\infty \sim m_\chi \left(1 + \frac{1}{2} u_\chi^2 \right), \quad (1.66)$$

and at a distance r from the star, it gets boosted to

$$E_\chi(r) = \frac{m_\chi}{\sqrt{B(r)}} \left(1 + \frac{1}{2} u_\chi^2 \right). \quad (1.67)$$

Therefore, the amount of energy that the DM must lose to be captured is

$$E_\chi^C(r) = \frac{1}{2} u_\chi^2 \frac{m_\chi}{\sqrt{B(r)}}. \quad (1.68)$$

$$\sim 0.6 \text{ GeV} \left(\frac{u_\chi}{270 \text{ km s}^{-1}} \right)^2 \left(\frac{m_\chi}{10^6 \text{ GeV}} \right) \left(\frac{0.5}{B(r)} \right)^{1/2}. \quad (1.69)$$

Hence, DM with a mass of 10^6 GeV with an initial velocity $u_\chi = 270 \text{ km s}^{-1}$, must lose 0.6 GeV of energy for it to be captured. This is of the same order as the maximum amount of energy that can be lost in a single scatter as seen in Fig. 1.2.

Given that q_0^{MAX} plates for $m_\chi \gg m_i$, it will be highly improbable that DM heavier than $\sim 10^6$ GeV loses enough energy in a single scatter to be captured. Single scatter capture is still possible as the DM velocity at infinity is not a fixed value, rather it follows by some distribution function. Therefore, the heavy DM could have a velocity close to zero at infinity, significantly reducing the amount of energy it needs to lose.

To account for this effect, we assume that the DM particles have a speed $u_\chi \ll 1$ at infinity that follows a Maxwell-Boltzmann (MB) distribution, Eq. 1.18. We can then define the probability density function (PDF) of the energy lost by the DM using the differential interaction rate through

$$\xi(q_0, E_\chi, \varepsilon_{F,i}) = \frac{1}{\Gamma^-(E_\chi)} \frac{d\Gamma^-}{dq_0}(q_0, E_\chi, \varepsilon_{F,i}), \quad (1.70)$$

where $\frac{d\Gamma^-}{dq_0}$ is the DM differential interaction rate, calculated in Appendix 1.3. The function ξ is defined for any $q_0 \geq 0$, however, kinematics dictates that the function is non-zero only for $q_0 \leq q_0^{\text{MAX}}$. Additionally, note that ξ depends on $B(r)$ through the ratio E_χ/m_χ , and for brevity we will simply write $\xi(q_0)$.

We can define the probability of losing at least an amount of energy $q_0 = \delta q_0$ in a single collision as

$$P_1(\delta q_0) = \int_{\delta q_0}^{\infty} dx \xi(x). \quad (1.71)$$

The probability of losing at least the same amount of energy after 2 collisions will then be

$$P_2(\delta q_0) = \int_{\delta q_0}^{\infty} dy \int_0^{\infty} dx \xi(x) \xi(y-x) \quad (1.72)$$

$$= P_1(\delta q_0) + \int_{\delta q_0}^{\infty} dy \int_0^y dx \xi(x) \xi(y-x) \quad (1.73)$$

$$= P_1(\delta q_0) + \int_0^{\delta q_0} dz P_1(\delta q_0 - z) \xi(z). \quad (1.74)$$

From this, we obtain the following recursive relation for the probabilities, P_N , of losing at least $q_0 = \delta q_0$ in N scatters,

$$P_{N+1}(\delta q_0) = P_N(\delta q_0) + \int_0^{\delta q_0} dz P_N(\delta q_0 - z) \xi(z). \quad (1.75)$$

In Fig. 1.8 we show how the probability functions P_1, \dots, P_5 changes based on the t dependence of the differential cross-section. We show results for $\sigma = \text{const.}$ (top

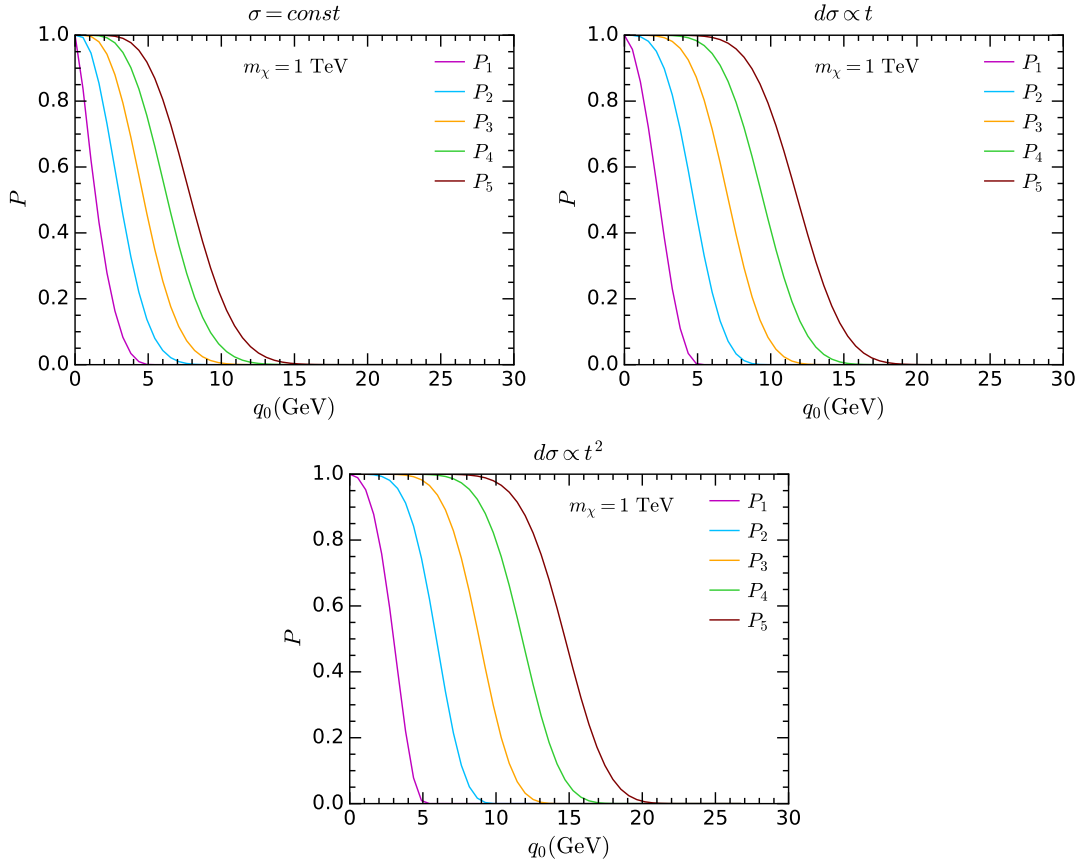


Figure 1.8: Probabilities to lose at least an amount of energy δq_0 after $1, \dots, 5$ scatterings, P_1, \dots, P_5 , as a function of the energy loss q_0 , assuming $B = 0.5$ and $\varepsilon_{F,n} = 400 \text{ MeV}$. Results are shown for different dependence on the cross-section on the Mandelstam variable t : constant DM-neutron cross-section (top left), $d\sigma \propto t$ (top right) and $d\sigma \propto t^2$ (bottom).

left), $d\sigma \propto t$ (top right) and $d\sigma \propto t^2$ (bottom), for fixed values of $B = 0.5$, $\varepsilon_{F,n} = 400 \text{ MeV}$.

To connect this back to the capture probability, we define the probability for a DM particle to be captured after exactly N interactions, c_N , to be $P_N(E_\chi^C) - P_{N-1}(E_\chi^C)$ averaged over the MB distribution of the initial velocity,

$$c_N(r) = \frac{1}{\int_0^\infty \frac{f_{\text{MB}}(u_\chi)}{u_\chi} du_\chi} \int_0^\infty \frac{f_{\text{MB}}(u_\chi)}{u_\chi} du_\chi \left[P_N \left(\frac{1}{2} \frac{m_\chi u_\chi^2}{\sqrt{B(r)}} \right) - P_{N-1} \left(\frac{1}{2} \frac{m_\chi u_\chi^2}{\sqrt{B(r)}} \right) \right], \quad (1.76)$$

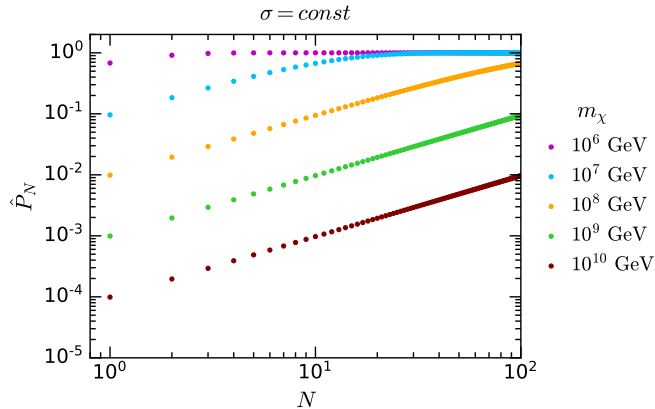


Figure 1.9: Cumulative probability \hat{P}_N for $B = 0.5$, $\varepsilon_{F,n} = 400$ MeV and for $\sigma = \text{const}$. as a function of the number of scatterings N for several DM masses.

where c_N depends on r through the dependence of P_N on $B(r)$ and $\varepsilon_{F,n}(r)$. Note that although our results will assume a Maxwell-Boltzmann velocity distribution, it is straightforward to generalise the results to any other DM velocity distribution. The cumulative probability \hat{P}_N that a DM particle is captured after N interactions with a total energy loss $\delta q_0 = E_\chi^C$ is then

$$\hat{P}_N(r) = \sum_{i=1}^N c_i = \frac{1}{\int_0^\infty \frac{f_{\text{MB}}(u_\chi)}{u_\chi} du_\chi} \int_0^\infty \frac{f_{\text{MB}}(u_\chi)}{u_\chi} du_\chi P_N \left(\frac{1}{2} \frac{m_\chi}{\sqrt{B(r)}} u_\chi^2 \right). \quad (1.77)$$

The resulting cumulative probability is shown as a function of the number of scatterings N in Fig. 1.9, for constant cross-section and several DM masses.

The cumulative probability \hat{P}_N for the above values of $B, \varepsilon_{F,n}$ is well approximated by the function⁶

$$\hat{P}_N \sim 1 - e^{-\frac{Nm_i^*}{m_\chi}}. \quad (1.78)$$

In particular, the probability that the DM is captured in a single scatter is

$$c_1 = \hat{P}_1 \sim 1 - e^{-\frac{m_i^*}{m_\chi}}. \quad (1.79)$$

From this, we see that c_1 will begin to significantly fall below unity for $m_\chi \gtrsim m_i^*$, and hence multiple scattering will only significantly reduce the capture rate for DM masses above m_i^* .

⁶Further discussion of the multi-scattering regime, and justification of this fitting function, can be found in Appendix C of Ref. [1].

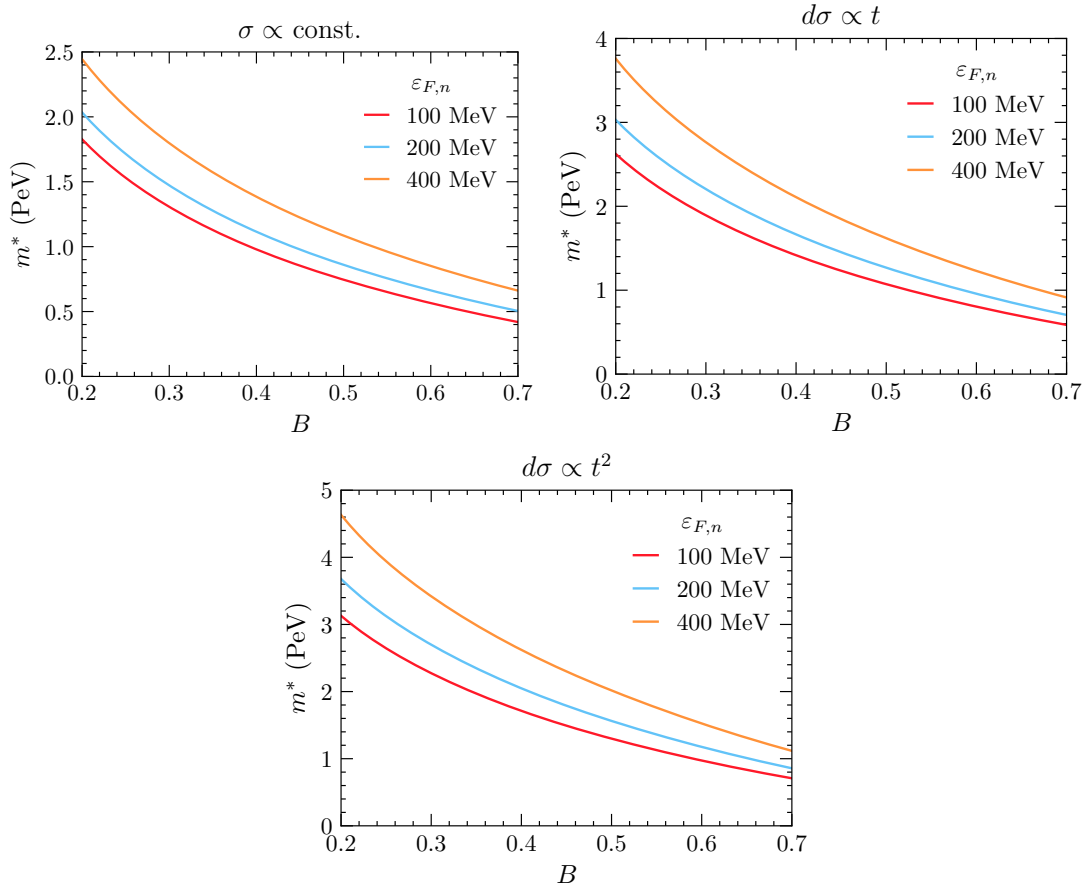


Figure 1.10: Value of m_n^* as a function of B for different values of $\varepsilon_{F,n}$, $\sigma = \text{const.}$ (top left), $d\sigma \propto t$ (top right) and $d\sigma \propto t^2$ (bottom).

To give an idea for how large the value of m_n^* will be, for neutron targets and the values $B = 0.5$ and $\varepsilon_{F,n} = 400$ MeV, we find

$$m^* = 1.08 \times 10^6 \text{ GeV}, \quad |\bar{\mathcal{M}}|^2 \propto t^0, \quad (1.80)$$

$$m^* = 1.62 \times 10^6 \text{ GeV}, \quad |\bar{\mathcal{M}}|^2 \propto t^1, \quad (1.81)$$

$$m^* = 2.01 \times 10^6 \text{ GeV}, \quad |\bar{\mathcal{M}}|^2 \propto t^2. \quad (1.82)$$

We illustrate how m_n^* varies with B and $\varepsilon_{F,n}$ in Fig. 1.10.

When the cross-section is small, $\sigma \ll \sigma_{\text{th}}$, such that we are in the optically thin regime, if the DM does not get captured in its initial scatter, then it will leave the star without interacting again. To account for this, the factor of c_1 should be included in the capture rate calculation, Eq. 1.26. However, as we have just seen, $c_1 \ll 1$ only for $m_\chi \gtrsim m_i^*$, which will always be significantly larger than the target mass and chemical potential. Therefore, multiple scattering is only important in

the regime where PB is negligible, and so a suitable approximation for the capture rate in this regime is

$$C_{\text{approx}}^* = \frac{4\pi}{v_*} \frac{\rho_\chi}{m_\chi} \text{Erf} \left(\sqrt{\frac{3}{2}} \frac{v_*}{v_d} \right) \int r^2 dr \frac{\sqrt{1 - B(r)}}{B(r)} \Omega^-(r) c_1(r), \quad (1.83)$$

with $\Omega^-(r)$ calculated as outlined in sections 1.4.1

1.5 Results

In this section, we present our results for the capture rate of fermionic DM scattering from neutrons within a NS in the zero temperature approximation. We calculate the capture rate only for scalar/pseudoscalar-scalar/pseudoscalar interactions between DM and neutrons, i.e. effective operators D1-D4 in Table ??, whose differential cross-sections depend only on the Mandelstam variable t and not on s . We use realistic radial profiles for the neutron number density, chemical potential, and relativistic corrections encoded in $B(r)$ as explained in section ??, obtained from the BS24 EoS for the configurations in Table ??.

To estimate the NS EoS impact on the DM capture rate computation, we numerically calculate C using the exact expression in the optically thin limit, Eq. 1.60, that properly accounts for gravitational focusing and Pauli blocking. In the optically thin regime that we are working in, the capture rate is proportional to the differential DM-neutron cross-section. Fig. 1.11 shows how this rate varies with the NS EoS for operators D1-D4 and the EoS configurations given in Table ??, and in turn with the NS mass and radius. The cross-section is normalised such that the capture rate in the intermediate mass range, which is unaffected by PB and multiple scattering, is equal to the geometric limit. It is worth remarking that cross-sections larger than the threshold cross-section should not be used in the optically thin limit, as this would result in capture rates larger than the geometric limit. To account for such large cross-sections, the optical depth of the NS must be accounted for as prescribed in Ref. [1]. Depending on the operator considered, going from the lightest to the heaviest NS can change the capture rate by a minimum of one order of magnitude, such as in the case of operators D1, D2 and D3 (at low DM mass), and up to 2 orders of magnitude, as in the case of operators D2 for large DM mass, and D4 in general.

At large DM mass, all operators show the same scaling with the DM mass. At $m_\chi \lesssim 1 \text{ GeV}$, a different picture arises as Pauli blocking leads to different suppressions of the capture rate for the different operators. However, we observe that the four operators give very similar results to those of Fig. 1.6, where we analysed the dependence of the capture rate on the momentum transfer t . We note that operator

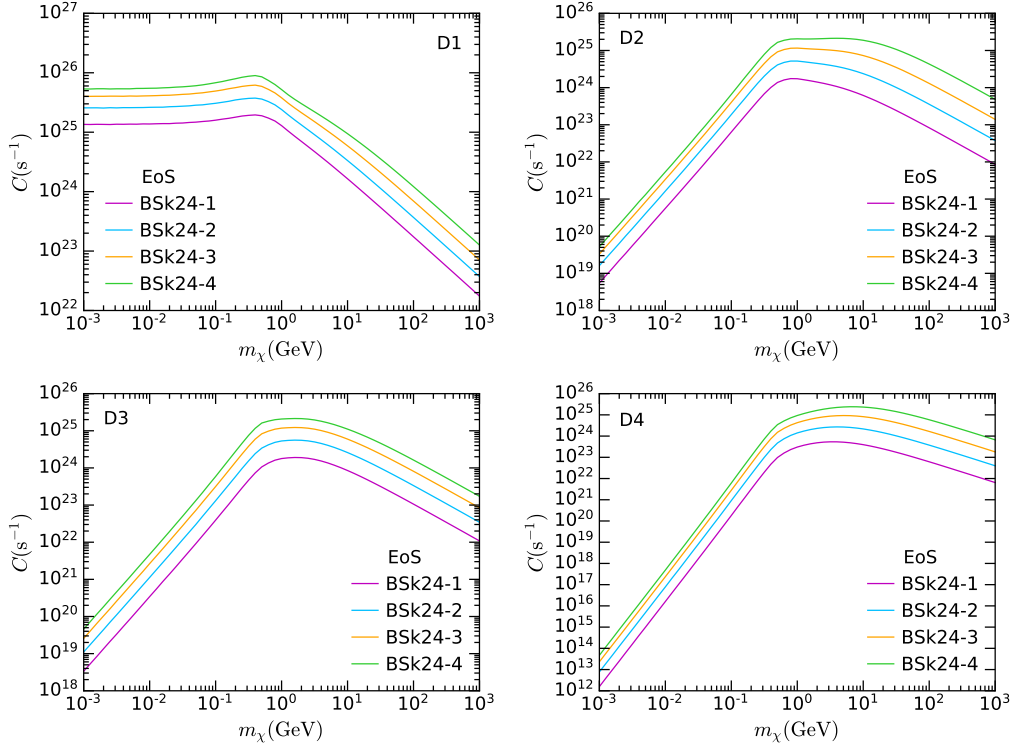


Figure 1.11: Capture rate in the optically thin limit as a function of the DM mass for $\sigma = \sigma_{\text{ref}} \sim 1.7 \times 10^{-45} \text{ cm}^2$ and the configurations of the EoS BSk24 given in Table ???. Rate calculated using the 4-dimensional integral in Eq. 1.60, that includes Pauli blocking but neglects the NS opacity and multiple scattering. Results are shown for the EFT operators D1 (top left), D2 (top right), D3 (bottom left) and D4 (bottom right) in Table ??.

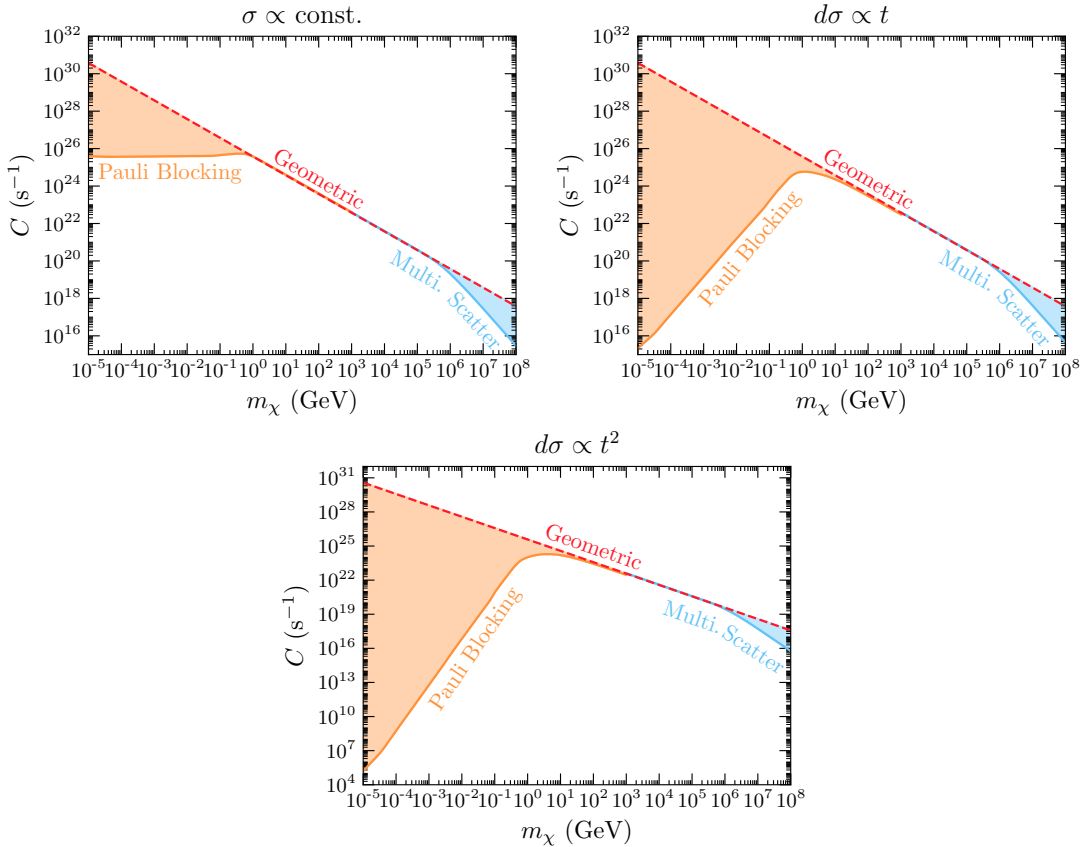


Figure 1.12: Capture rate for constant cross-section (top left), $d\sigma \propto t$ (top right) and $d\sigma \propto t^2$ (bottom), for $\sigma = \sigma_{\text{ref}} \sim 1.7 \times 10^{-45} \text{ cm}^2$ and NS EoS configuration BSk24-2. These plots extent the mass range of those in Fig. 1.6 to large DM masses.

D1, which contains in its squared matrix element a term independent of t , gives a result that is very similar to that of $\sigma = \text{const.}$ Operators D2 and D3, for which $|\bar{\mathcal{M}}|^2$ does not include terms independent of t , but rather terms proportional to t and t^2 , yield very similar results to that of $d\sigma \propto t$. Overall, we conclude that the lowest power of the transferred momentum determines the mass scaling of the capture rate at low DM mass. This result holds true for matrix elements that depend also on s .

In Fig. 1.12, we show the capture rate for a broad DM mass range, spanning 13 orders of magnitude from $m_\chi = 10 \text{ keV}$ to $m_\chi = 10^8 \text{ GeV}$, including all three of the mass regimes we have discussed in the previous sections, for $d\sigma \propto \text{const.}$ (first row), t^1 (second row) and t^2 (third row). The orange line indicates the capture rate calculated in the optically thin limit using the 4-dimensional integration in Eq. 1.59 that accounts for Pauli blocking. At large DM masses, Pauli suppression plays no role and the capture rate approaches the geometric limit (dashed red line). We

also show in Fig. 1.12 the effect of the inclusion of multiple scattering in the light blue line, which becomes relevant at $m_\chi \sim 10^6$ GeV. At $m_\chi \sim 10^5$ GeV that line matches the geometric limit as expected from the chosen value of the cross-section $\sigma = \sigma_{\text{ref}}$. At larger DM masses, $m_\chi \gtrsim 10^6$ GeV, multiple scatterings are required for the DM to be captured, hence an additional suppression factor of $1/m_\chi$ arises, as given in Eq. 1.83. Therefore, the capture rate becomes increasingly smaller than C_{geom} (light blue shaded area).

Comparing the plots for different t^n dependence, we can see that increasing the power of n has a small effect on the mass scale where the various suppressions become relevant. For example, comparing the light blue lines between the three figures, we see that the change of slope from the onset of multiple scattering moves slightly further to the right for larger n . This is a consequence of the fact that larger powers of n result in larger energy transfer (see, for example, Fig. A.2), leading to a larger capture probability c_1 and hence a larger m_i^* . However, the qualitative behaviour is the same for all choices of $d\sigma$: the suppression of the capture rate is primarily due to Pauli blocking at low mass and multiple scattering effects (i.e. a low capture probability) at large masses.

1.6 Summary

In this chapter, we have improved and extended the existing framework used to calculate the DM capture rate in the Sun to be compatible with compact objects, relaxing the simplifying assumptions that have previously been made. Specifically, we have derived exact expressions for the capture rate that correctly incorporate relativistic kinematics, gravitational focusing, Pauli blocking, and multiple-scattering effects. We also properly incorporate the internal structure of the star, consistently calculating the radial profiles of the EoS-dependent parameters and the general relativistic corrections, by solving the Tolman-Oppenheimer-Volkoff equations.

This new formalism was applied to neutron stars to highlight the features of the formalism mentioned above. Neutron stars (and compact objects in general) are composed of strongly degenerate matter, resulting in significant Pauli blocking of scattering interactions when the dark matter is light, $m_\chi \lesssim m_i$, suppressing the capture rate by several orders of magnitude. By including the radial dependence of the chemical potential in our calculations, we correctly account for Pauli suppression at any point in the star. However, note that the chemical potential is dependent on the EoS assumption.

For very large DM masses, $m_\chi \gtrsim 10^6$ GeV, the energy lost in a single collision will be insufficient for it to be captured. Hence, the DM must scatter multiple times within an orbit to be captured, or else it simply leaves the star. To correctly

compute the DM capture probability due to multiple scattering, we have derived, for the first time, an exact equation for the DM interaction rate in degenerate matter, and used that result to compute the differential capture rate as a function of the DM energy loss. This enables us to compute the cumulative probability that a DM particle is captured after multiple interactions, by averaging over the initial DM velocity distribution.

Although we have framed our results in terms of the scattering of DM from neutron targets in neutron star, it is straightforward to obtain the capture rate for DM scattering from any other degenerate species in compact objects. In the next chapter, we apply this formalism to DM scattering off the leptonic components of NSs, as well as the degenerate electrons within WDs.

A

Derivation of Dark Matter Interaction Rates in Degenerate Media

A.1 General Interaction Rates

The most general form of the interaction rate, following Ref. [14], can be written as

$$\Gamma = \int \frac{d^3 k'}{(2\pi)^3} \frac{1}{(2E_\chi)(2E'_\chi)(2m_i)(2m_i)} \Theta(E'_\chi - m_\chi) \Theta(\pm q_0) S(q_0, q), \quad (\text{A.1})$$

$$S(q_0, q) = 2 \int \frac{d^3 p}{(2\pi)^3} \int \frac{d^3 p'}{(2\pi)^3} \frac{m_i^2}{E_i E'_i} |\bar{\mathcal{M}}|^2 (2\pi)^4 \delta^4(k_\mu + p_\mu - k'_\mu - p'_\mu) \\ \times f_{\text{FD}}(E_i)(1 - f_{\text{FD}}(E'_i)) \Theta(E_i - m_i) \Theta(E'_i - m_i), \quad (\text{A.2})$$

The δ -function can be used to perform the $d^3 p'$ integrations, leaving

$$S(q_0, q) = \frac{1}{2\pi^2} \int d^3 p \frac{m_i^2}{E_i E'_i} |\bar{\mathcal{M}}|^2 \delta(q_0 + E_i - E'_i) f_{\text{FD}}(E_i)(1 - f_{\text{FD}}(E'_i)) \\ \times \Theta(E_i - m_i) \Theta(E'_i - m_i). \quad (\text{A.3})$$

After this, the final state target energy is fixed to

$$E'_i(E_i, q, \theta) = \sqrt{m_i^2 + (\vec{p} + \vec{q})^2} \quad (\text{A.4})$$

$$= \sqrt{E_i^2 + q^2 + 2qp \cos \theta} > m_i, \quad \forall p, q, \theta, |\cos \theta| < 1, \quad (\text{A.5})$$

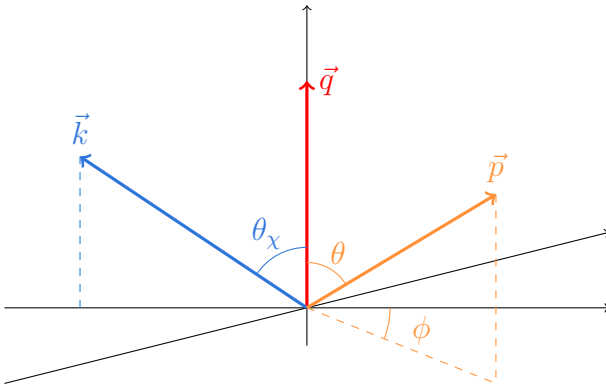


Figure A.1: Schematic of kinematics for dark matter interacting with a target in the frame of the star. We set the momentum transfer to lie along the z -axis with the initial momenta defined relative to it.

where θ is the angle between the target initial momentum and the transferred momentum, \vec{q} , that is defined below. To perform the remaining integrals, we write $d^3p = pE_idE_i d\cos\theta d\phi$. The kinematics of this interaction are depicted in Fig. A.1, where the incoming momenta are defined relative to the momentum transfer that is set to lie along the z -axis. In doing so, we must account for the fact that in this frame we cannot assume all three of the vectors are coplanar, and assign the additional azimuthal angle ϕ to the target momentum.

In general, the squared matrix elements we are interested in can be expressed as polynomials in the Mandelstam variables s and t , such that

$$|\overline{\mathcal{M}}|^2 = \sum_{n,m} \alpha_{n,m} t^n s^m. \quad (\text{A.6})$$

Writing $s = m_\chi^2 + m_i^2 + 2E_\chi E_i - 2\vec{p} \cdot \vec{k}$, the quantity $\vec{k} \cdot \vec{p}$ is obtained by analysing the kinematics of the interaction. From the diagram in Fig. A.1, we can write the initial momenta as

$$\vec{k} = (k \sin \theta_\chi, 0, k \cos \theta_\chi), \quad (\text{A.7})$$

$$\vec{p} = (p \sin \theta \cos \phi, p \sin \theta \sin \phi, p \cos \theta). \quad (\text{A.8})$$

The angles can then be expressed in terms of the other kinematic quantities by

noting that

$$E'_\chi = \sqrt{m_\chi^2 + (\vec{k} - \vec{q})}, \quad (\text{A.9})$$

$$\implies (E_\chi - q_0)^2 = m_\chi^2 + (k^2 + q^2 - 2kq \cos \theta_\chi) \quad (\text{A.10})$$

$$\implies \cos \theta_\chi = \frac{q^2 - q_0^2 + 2E_\chi q_0}{2q \sqrt{E_\chi^2 - m_\chi^2}}, \quad (\text{A.11})$$

$$E'_i = \sqrt{m_i^2 + (\vec{p} + \vec{q})}, \quad (\text{A.12})$$

$$(\text{A.13})$$

for the dark matter angle, and

$$\implies (E_i + q_0)^2 = m_i^2 + (p^2 + q^2 + 2pq \cos \theta) \quad (\text{A.14})$$

$$\implies \cos \theta = \frac{q_0^2 - q^2 + 2E_i q_0}{2q \sqrt{E_i^2 - m_i^2}} \quad (\text{A.15})$$

for the target angle. These result in

$$\vec{k} \cdot \vec{p} = kp \sin \theta_\chi \sin \theta \cos \phi + kp \cos \theta_\chi \cos \theta \quad (\text{A.16})$$

$$\begin{aligned} &= kp \left[\sqrt{1 - \frac{(q^2 - q_0^2 + 2E_\chi q_0)^2}{4q^2(E_\chi^2 - m_\chi^2)}} \sqrt{1 - \frac{(q_0^2 - q^2 + 2E_i q_0)^2}{4q^2(E_i^2 - m_i^2)}} \cos \phi \right. \\ &\quad \left. + \frac{(q^2 - q_0^2 + 2E_\chi q_0)(q_0^2 - q^2 + 2E_i q_0)}{4q^2 \sqrt{E_\chi^2 - m_\chi^2} \sqrt{E_i^2 - m_i^2}} \right] \end{aligned} \quad (\text{A.17})$$

$$\begin{aligned} &= \frac{(q^2 - q_0^2 + 2E_\chi q_0)(q_0^2 - q^2 + 2E_i q_0)}{4q^2} \\ &\quad + \sqrt{E_\chi^2 - m_\chi^2 - \frac{(q^2 - q_0^2 + 2E_\chi q_0)^2}{4q^2}} \sqrt{E_i^2 - m_i^2 - \frac{(q_0^2 - q^2 + 2E_i q_0)^2}{4q^2}} \cos \phi. \end{aligned} \quad (\text{A.18})$$

This makes explicit that s is now a function of the azimuthal angle ϕ .

We then use the remaining delta function to integrate over θ , giving rise to a step function $\Theta(1 - \cos^2 \theta(q, q_0, E_i))$, leaving the

$$S(q_0, q) = \alpha t^n \frac{m_i^2}{2\pi^2 q} \int dE_i d\phi s^m f_{\text{FD}}(E_i) (1 - f_{\text{FD}}(E_i + q_0)) \Theta(E_i) \Theta(1 - \cos^2 \theta). \quad (\text{A.19})$$

It will be more convenient to work with the kinetic energies of the targets rather than their total energies, as we are only interested in elastic scattering. From here on out, E_i will refer to the kinetic energy of the target, i.e. $E_i \rightarrow E_i + m_i$.

This is compensated by using the Fermi kinetic energy in the FD distributions, $\varepsilon_{F,i} = \mu_{F,i} - m_i$.

The ϕ integrals can be easily computed for a given power of s , in general resulting in a messy function of the kinematic variables. However, we know that they will always be a polynomial of degree m , and so to make this explicit while keeping things as tidy as possible, we define the polynomials $\mathcal{U}_m(q^2, q_0, E_\chi, E_i)$ as

$$\mathcal{U}_m = \frac{q^{2m}}{2\pi} \int_0^{2\pi} d\phi s^m = \sum_r \mathcal{V}_{m,r} E_i^r \quad (\text{A.20})$$

where the coefficients of the polynomial, $\mathcal{V}_{m,r}$, are functions of q^2, q_0 , and E_χ . The response function is then

$$S(q_0, q) = \alpha t^n \frac{m_i^2}{\pi q} \int dE_i f_{\text{FD}}(E_i) (1 - f_{\text{FD}}(E_i + q_0)) \frac{\mathcal{U}_m}{q^{2m}} \Theta(E_i) \Theta(1 - \cos^2 \theta). \quad (\text{A.21})$$

Therefore, the integrals we are interested in computing are over the FD distributions, which we call

$$\mathcal{F}_r(E_i, q_0) = \int dE_i E_i^r f_{\text{FD}}(E_i) (1 - f_{\text{FD}}(E_i + q_0)). \quad (\text{A.22})$$

To proceed, make the change to the dimensionless variables

$$x = \frac{E_i - \varepsilon_{F,i}}{T_\star}, \quad z = \frac{q_0}{T_\star}, \quad (\text{A.23})$$

which we can use to write

$$\mathcal{F}_r(E_i, q_0) = T_\star \int dx (\varepsilon_{F,i} + T_\star x)^r f_{\text{FD}}(x) f_{\text{FD}}(-x - z) \quad (\text{A.24})$$

$$= T_\star \int dx \sum_{j=0}^r \binom{r}{j} T_\star^j x^j \varepsilon_{F,i}^{r-j} f_{\text{FD}}(x) f_{\text{FD}}(-x - z) \quad (\text{A.25})$$

$$= \sum_{j=0}^r T_\star^{j+1} \binom{r}{j} \varepsilon_{F,i}^{r-j} \int dx x^j f_{\text{FD}}(x) f_{\text{FD}}(-x - z) \quad (\text{A.26})$$

$$= \sum_{j=0}^r \binom{r}{j} \varepsilon_{F,i}^{r-j} \int dE_i (E_i - \varepsilon_{F,i})^j f_{\text{FD}}(E_i) f_{\text{FD}}(-E_i - q_0) \quad (\text{A.27})$$

$$= \sum_{j=0}^r \binom{r}{j} \varepsilon_{F,i}^{r-j} (-1)^j \frac{q_0^{j+1}}{j+1} g_j \left(\frac{E_i - \varepsilon_{F,i}}{q_0} \right), \quad \text{for } T_\star \rightarrow 0, \quad (\text{A.28})$$

where the final line holds in the zero-temperature approximation in which the FD distributions become Θ -functions, allowing the integrals to be expressed in terms of the function

$$g_j(x) = \begin{cases} 1, & x > 0 \\ 1 - (-x)^{j+1}, & -1 < x < 0 \\ 0, & x < -1 \end{cases} \quad (\text{A.29})$$

The integration range for E_i is obtained from the two Θ -functions. There are two cases to be considered, $t < 0$ and $t > 0$. In the former case, the range become $E_i^{t^-} < E_i < \infty$ and for the latter $0 < E_i < E_i^{t^+}$. These integration bounds are obtained from Eq. A.15, by settting $\cos \theta = 1$, and are given by

$$E_i^{t^-} = -\left(m_i + \frac{q_0}{2}\right) + \sqrt{\left(m_i + \frac{q_0}{2}\right)^2 + \left(\frac{\sqrt{q^2 - q_0^2}}{2} - \frac{m_i q_0}{\sqrt{q^2 - q_0^2}}\right)^2} \quad (\text{A.30})$$

$$E_i^{t^+} = -\left(m_i + \frac{q_0}{2}\right) + \sqrt{\left(m_i + \frac{q_0}{2}\right)^2 - \left(\frac{\sqrt{q_0^2 - q^2}}{2} + \frac{m_i q_0}{\sqrt{q_0^2 - q^2}}\right)^2}. \quad (\text{A.31})$$

These are both the same root of Eq. A.15, but with an interchange of $t \leftrightarrow -t$. We denote the response function for $t < 0$ as S^- and for $t > 0$ as S^+ . For S^- we have

$$S_m^- = \alpha t^n \frac{m_i^2}{\pi q^{2m+1}} \sum_{r=0}^m \mathcal{V}_{m,r} \int_{E_i^{t^-}}^{\infty} dE_i E_i^r f_{\text{FD}}(E_i) (1 - f_{\text{FD}}(E_i + q_0)) \quad (\text{A.32})$$

$$= \alpha t^n \frac{m_i^2}{\pi q^{2m+1}} \sum_{r=0}^m \mathcal{V}_{m,r} \sum_{j=0}^r \binom{r}{j} \varepsilon_{F,i}^{r-j} \int_{E_i^{t^-}}^{\infty} dE_i (E_i - \varepsilon_{F,i})^j f_{\text{FD}}(E_i) f_{\text{FD}}(-E_i - q_0) \quad (\text{A.33})$$

$$= \alpha t^n \frac{m_i^2}{\pi q^{2m+1}} \sum_{r=0}^m \mathcal{V}_{m,r} \sum_{j=0}^r \binom{r}{j} \varepsilon_{F,i}^{r-j} \frac{(-1)^j q_0^{j+1}}{j+1} \left[1 - g_j \left(\frac{E_i^{t^-} - \varepsilon_{F,i}}{q_0} \right) \right] \quad (\text{A.34})$$

$$= \alpha t^n \frac{m_i^2}{\pi q^{2m+1}} \sum_{r=0}^m \mathcal{V}_{m,r} \sum_{j=0}^r \binom{r}{j} \varepsilon_{F,i}^{r-j} \frac{(-1)^j q_0^{j+1}}{j+1} h_j \left(\frac{E_i^{t^-} - \varepsilon_{F,i}}{q_0} \right), \quad (\text{A.35})$$

while for S^+ the logic is

$$S_m^+ = \alpha t^n \frac{m_i^2}{\pi q^{2m+1}} \sum_{r=0}^m \mathcal{V}_{m,r} \int_0^{E_i^{t^+}} dE_i E_i^r f_{\text{FD}}(E_i) (1 - f_{\text{FD}}(E_i + q_0)) \quad (\text{A.36})$$

$$= \alpha t^n \frac{m_i^2}{\pi q^{2m+1}} \sum_{r=0}^m \mathcal{V}_{m,r} \sum_{j=0}^r \binom{r}{j} \varepsilon_{F,i}^{r-j} \int_0^{E_i^{t^+}} dE_i (E_i - \varepsilon_{F,i})^j f_{\text{FD}}(E_i) f_{\text{FD}}(-E_i - q_0) \quad (\text{A.37})$$

$$= \alpha t^n \frac{m_i^2}{\pi q^{2m+1}} \sum_{r=0}^m \mathcal{V}_{m,r} \sum_{j=0}^r \binom{r}{j} \varepsilon_{F,i}^{r-j} \frac{(-1)^j q_0^{j+1}}{j+1} \left[g_j \left(\frac{E_i^{t^+} - \varepsilon_{F,i}}{q_0} \right) - g_j \left(\frac{-\varepsilon_{F,i}}{q_0} \right) \right] \quad (\text{A.38})$$

$$= -\alpha t^n \frac{m_i^2}{\pi q^{2m+1}} \sum_{r=0}^m \mathcal{V}_{m,r} \sum_{j=0}^r \binom{r}{j} \varepsilon_{F,i}^{r-j} \frac{(-1)^j q_0^{j+1}}{j+1} h_j \left(\frac{E_i^{t^+} - \varepsilon_{F,i}}{q_0} \right) \quad \text{for } q_0 < 0, \quad (\text{A.39})$$

with

$$h_j(x) = \begin{cases} 0, & x > 0 \\ (-x)^{j+1}, & -1 < x < 0 \\ 1, & x < -1 \end{cases} \quad (\text{A.40})$$

The final step of the S^+ calculation holds only for up-scattering of the DM, i.e. $q_0 < 0$.

For matrix elements that are polynomials in s and t , the full response function is simply the sum of the n and m , giving

$$S^- = \sum_{n,m} \alpha_{n,m} t^n \frac{m_i^2}{\pi q^{2m+1}} \sum_{r=0}^m \mathcal{V}_{m,r} \sum_{j=0}^r \binom{r}{j} \varepsilon_{F,i}^{r-j} \frac{(-1)^j q_0^{j+1}}{j+1} h_j \left(\frac{E_i^{t^-} - \varepsilon_{F,i}}{q_0} \right) \quad (\text{A.41})$$

$$S^+ = - \sum_{n,m} \alpha_{n,m} t^n \frac{m_i^2}{\pi q^{2m+1}} \sum_{r=0}^m \mathcal{V}_{m,r} \sum_{j=0}^r \binom{r}{j} \varepsilon_{F,i}^{r-j} \frac{(-1)^j q_0^{j+1}}{j+1} h_j \left(\frac{E_i^{t^+} - \varepsilon_{F,i}}{q_0} \right) \quad (\text{A.42})$$

A.2 Elsatic Scattering

A.2.1 Down-scattering Rate

Returning to the scattering rate, we first look at the case of down-scattering, where the DM loses energy, $q_0 > 0$. In this case, the interaction rate is given by

$$\begin{aligned} \Gamma^-(E_\chi) = & \int \frac{d \cos \theta_\chi k'^2 dk'}{64\pi^3 E_\chi E'_\chi} \Theta(E_\chi - q_0 - m_\chi) \Theta(q_0) \sum_{n,m} \frac{\alpha_{n,m} t^n}{q^{2m+1}} \\ & \times \sum_{r=0}^m \mathcal{V}_{m,r} \sum_{j=0}^r \binom{r}{j} \varepsilon_{F,i}^{r-j} \frac{(-1)^j q_0^{j+1}}{j+1} h_j \left(\frac{E_i^{t^-} - \varepsilon_{F,i}}{q_0} \right) \end{aligned} \quad (\text{A.43})$$

Change variables to q_0 and q through

$$q_0 = E_\chi - \sqrt{k'^2 + m_\chi^2}, \quad (\text{A.44})$$

$$q^2 = k^2 + k'^2 - 2kk' \cos \theta_\chi, \quad (\text{A.45})$$

$$\implies dk' d \cos \theta_\chi = \frac{E'_\chi q}{kk'^2} dq_0 dq \quad (\text{A.46})$$

To further simplify the notation we introduce $t_E = -t = q^2 - q_0^2$, $dq = dt_E/(2q)$, and exchange the q -integral for

$$\implies dk' d \cos \theta_\chi = \frac{E'_\chi}{2kk'^2} dq_0 dt_E, \quad (\text{A.47})$$

giving the interaction rate as

$$\begin{aligned} \Gamma^-(E_\chi) = & \frac{1}{128\pi^3 E_\chi k} \int_0^{E_\chi - m_\chi} dq_0 \int dt_E \sum_{n,m} \frac{\alpha_{n,m} (-1)^n t_E^n}{(t_E + q_0^2)^{m+\frac{1}{2}}} \\ & \times \sum_{r=0}^m \mathcal{V}_{m,r} \sum_{j=0}^r \binom{r}{j} \varepsilon_{F,i}^{r-j} \frac{(-1)^j q_0^{j+1}}{j+1} h_j \left(\frac{E_i^{t^-} - \varepsilon_{F,i}}{q_0} \right) \end{aligned} \quad (\text{A.48})$$

$$\begin{aligned} = & \sum_{n,m} \frac{(-1)^n \alpha_{n,m}}{128\pi^3 E_\chi k} \int_0^{E_\chi - m_\chi} dq_0 \int \frac{dt_E t_E^n}{(t_E + q_0^2)^{m+\frac{1}{2}}} \\ & \times \sum_{r=0}^m \mathcal{V}_{m,r} \sum_{j=0}^r \binom{r}{j} \varepsilon_{F,i}^{r-j} \frac{(-1)^j q_0^{j+1}}{j+1} h_j \left(\frac{E_i^{t^-} - \varepsilon_{F,i}}{q_0} \right). \end{aligned} \quad (\text{A.49})$$

There are then two main cases to consider; when $h_j(x)$ is unity or when it is not. We denote the t_E integrand in the former case as f_1 and f_2 for the latter, given explicitly as

$$f_1^{(m,n)}(t_E) = \frac{t_E^n}{(t_E + q_0^2)^{m+\frac{1}{2}}} \sum_{r=0}^m \mathcal{V}_{m,r} \sum_{j=0}^r \binom{r}{j} \varepsilon_{F,i}^{r-j} \frac{(-1)^j q_0^{j+1}}{j+1}, \quad (\text{A.50})$$

$$f_2^{(m,n)}(t_E) = \frac{-t_E^n}{(t_E + q_0^2)^{m+\frac{1}{2}}} \sum_{r=0}^m \mathcal{V}_{m,r} \sum_{j=0}^r \binom{r}{j} \varepsilon_{F,i}^{r-j} \frac{1}{j+1} \left(E_i^{t^-} - \varepsilon_{F,i} \right)^{j+1}, \quad (\text{A.51})$$

where we suppress the explicit dependence on the other variables for brevity. We encode the integrals over t_E within an operator

$$\begin{aligned} \mathcal{I}_{n,m}(f^{(m,n)}(t), t_1^+, t_2^+, t_1^-, t_2^-) &= \sum_{i=1,2} \sum_{j=1,2} \left(F^{(m,n)}(t_i^+) - F^{(m,n)}(t_j^-) \right) \\ &\quad \times \Theta(t_{3-i}^+ - t_i^+) \Theta(t_i^+ - t_j^-) \Theta(t_j^- - t_{3-j}^-), \end{aligned} \quad (\text{A.52})$$

$$F^{(m,n)}(t) = \int dt f^{(m,n)}(t). \quad (\text{A.53})$$

The full interaction rate is then written as

$$\begin{aligned} \Gamma^-(E_\chi) &= \sum_{n,m} \frac{(-1)^n \alpha_{n,m}}{128\pi^3 E_\chi k} \int_0^{E_\chi - m_\chi} dq_0 \\ &\quad \times \left[\mathcal{I}_{n,m} \left(f_1^{(m,n)}(t), t_E^+, t_{\mu^-}^+, t_E^-, t_{\mu^-}^- \right) \Theta(\varepsilon_{F,i} - q_0) \right. \\ &\quad + \mathcal{I}_{n,m} \left(f_2^{(m,n)}(t), t_E^+, t_{\mu^+}^+, t_E^-, t_{\mu^+}^- \right) \Theta(\varepsilon_{F,i} - q_0) \\ &\quad + \mathcal{I}_{n,m} \left(f_2^{(m,n)}(t), t_E^+, t_{\mu^-}^-, t_E^-, t_{\mu^+}^- \right) \Theta(\varepsilon_{F,i} - q_0) \\ &\quad \left. + \mathcal{I}_{n,m} \left(f_2^{(m,n)}(t), t_E^+, t_{\mu^+}^+, t_E^-, t_{\mu^+}^- \right) \Theta(q_0 - \varepsilon_{F,i}) \right], \end{aligned} \quad (\text{A.54})$$

where the t_E integration limits are

$$t_E^\pm = 2 \left[E_\chi(E_\chi - q_0) - m_\chi^2 \pm k \sqrt{(E_\chi - q_0)^2 - m_\chi^2} \right], \quad (\text{A.55})$$

$$\begin{aligned} t_{\mu^+}^\pm &= 2 [\varepsilon_{F,i}(\varepsilon_{F,i} + q_0) + m_i(2\varepsilon_{F,i} + q_0) \\ &\quad \pm \sqrt{(\varepsilon_{F,i}(\varepsilon_{F,i} + q_0) + m_i(2\varepsilon_{F,i} + q_0))^2 - m_i^2 q_0^2}], \end{aligned} \quad (\text{A.56})$$

$$\begin{aligned} t_{\mu^-}^\pm &= 2 [\varepsilon_{F,i}(\varepsilon_{F,i} - q_0) + m_i(2\varepsilon_{F,i} - q_0) \\ &\quad \pm \sqrt{(\varepsilon_{F,i}(\varepsilon_{F,i} - q_0) + m_i(2\varepsilon_{F,i} - q_0))^2 - m_i^2 q_0^2}], \end{aligned} \quad (\text{A.57})$$

All interaction rate spectra will have an endpoint at $q_0 = q_0^{\text{MAX}}$, the maximum amount of energy that can be lost in a single interaction. The value of q_0^{MAX} is shown in the left panel of Fig. 1.2 as a function of B in the case of large DM mass ($m_\chi = 1 \text{ TeV}$), for several values of $\varepsilon_{F,n}$. The endpoint can be found as the minimum between the DM kinetic energy and the root of one of the following two equations

$$t_E^- = t_{\mu^+}^+, \quad (\text{A.58})$$

$$t_E^+ = t_{\mu^+}^-. \quad (\text{A.59})$$

Only one of these equations will have a positive root for a given choice of m_χ , $\varepsilon_{F,n}$ and E_χ . For $m_\chi \gg m_i$, the second equation never has a solution, and the solution of the first equation is always much lower than the kinetic energy. This results in the value of q_0^{MAX} becoming independent of m_χ in this mass range.

The shape of the differential interaction rate depends very weakly on m_χ and B for $m_\chi \gg m_i$ and $m_\chi \ll m_i$, as seen by plotting it as a function of $q_0^{\text{norm}} = q_0/q_0^{\text{MAX}}$. Therefore, we use as a reference $m_\chi = 1 \text{ TeV}$ (left) and $m_\chi = 10 \text{ MeV}$ (right), $B = 0.5$, and show the normalised differential interaction rates in Fig. A.2 for $n = 0, 1, 2$, and neutron targets. We observe in the left panels that for $n = 0$ interaction rates are flat (or peaked, depending on $\varepsilon_{F,n}$) at low energy and suppressed at high energies, while for $n = 1, 2$ the profiles become peaked at higher and higher energies. Conversely, for $m_\chi = 10 \text{ MeV}$ the peak of the spectrum is shifted to lower energies with increasing power of t ($d\sigma \propto t^n$).

A.3 Up-scattering Rate

We now treat the case of $q_0 < 0$ applicable to up scattering and evaporation. Focusing on s -independent matrix elements for the moment, the response function is

$$S_{\text{up}}^-(q_0, q) = \frac{m_i^2}{\pi q} \int_{E_i^{t-}}^{\infty} f_{\text{FD}}(E_i) (1 - f_{\text{FD}}(E_i - |q_0|)) \quad (\text{A.60})$$

and evaluate the integral, now with $q_0 < 0$. If we attempt to take the $T_\star \rightarrow 0$ limit as before, we find that there is no overlap of the FD distributions and the result vanishes. Instead, we keep the leading order thermal corrections, i.e. terms of order $e^{-|q_0|/T_\star}$. The result is

$$\mathcal{F}_0(E_i, -|q_0|) = \frac{T_\star e^{-|q_0|/T_\star}}{1 - e^{-|q_0|/T_\star}} \left[\log \left(1 + e^{(E_i - \varepsilon_{F,i})/T_\star} \right) - \log \left(1 + e^{(E_i - |q_0| - \varepsilon_{F,i})/T_\star} \right) \right], \quad (\text{A.61})$$

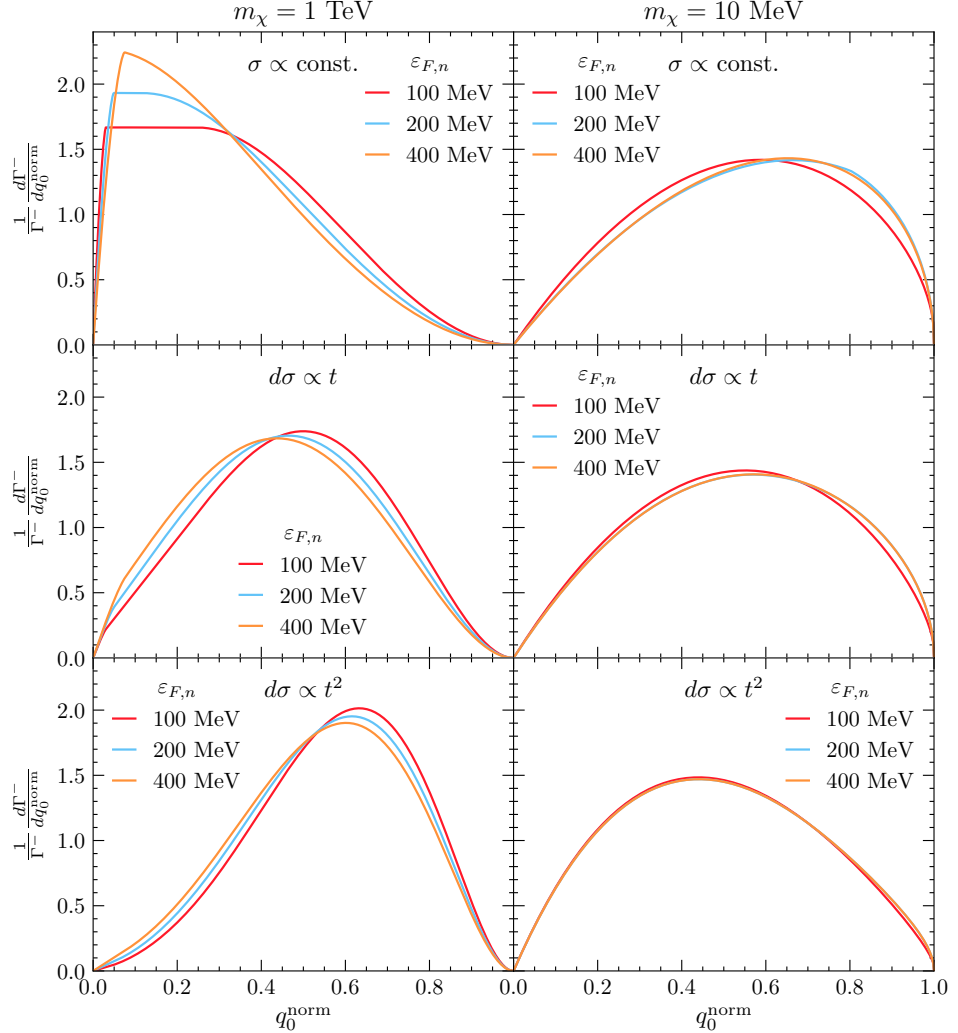


Figure A.2: Normalised differential interaction rates, $\frac{1}{\Gamma} \frac{d\Gamma^-}{dq_0^n \text{norm}}$, as a function of $q_0^n \text{norm}$ for different values of $\varepsilon_{F,n}$, with $m_\chi = 1 \text{ TeV}$ (left panels) $m_\chi = 10 \text{ MeV}$ (right panels) and $B = 0.5$. Top row: $n = 0$, middle row: $n = 1$, bottom row: $n = 2$.

where after taking $T_\star \rightarrow 0$ we recognise three regions of interest

$$\lim_{T_\star \rightarrow 0} T_\star \mathcal{F}_0(E_i, -|q_0|) = \begin{cases} \frac{|q_0| e^{-|q_0|/T_\star}}{1 - e^{-|q_0|/T_\star}}, & E_i > \varepsilon_{F,i} + |q_0| \\ \frac{(E_i - \varepsilon_{F,i}) e^{-|q_0|/T_\star}}{1 - e^{-|q_0|/T_\star}}, & \varepsilon_{F,i} + |q_0| > E_i > \varepsilon_{F,i} \\ 0, & \varepsilon_{F,i} > E_i \end{cases} \quad (\text{A.62})$$

and we can write this as

$$\lim_{T_\star \rightarrow 0} T_\star \mathcal{F}_0(E_i, -|q_0|) = \frac{|q_0| e^{-|q_0|/T_\star}}{1 - e^{-|q_0|/T_\star}} h_0 \left(\frac{\varepsilon_{F,i} - E_i}{q_0} \right). \quad (\text{A.63})$$

The response function for upscattering is then

$$S_{\text{up}}^-(q_0, q) = \frac{m_i^2 q_0}{\pi q} \frac{e^{-|q_0|/T_\star}}{e^{-|q_0|/T_\star} - 1} \left[1 - h_0 \left(\frac{E_i^{t^-} - \varepsilon_{F,i}}{q_0} \right) \right] \quad (\text{A.64})$$

$$= \frac{m_i^2 q_0}{\pi q} \frac{e^{-|q_0|/T_\star}}{e^{-|q_0|/T_\star} - 1} g_0 \left(\frac{\varepsilon_{F,i} - E_i^{t^-}}{q_0} \right), \quad (\text{A.65})$$

leading to the corresponding up-scattering rate being

$$\Gamma_{\text{up}}^-(E_\chi) = \int \frac{k'^2 d \cos \theta dk'}{64\pi^2 m_i^2 E_\chi E'_\chi} |\bar{\mathcal{M}}|^2 \Theta(E_\chi + |q_0| - m_\chi) \Theta(q_0) S_{\text{up}}^-(q_0, q) \quad (\text{A.66})$$

$$= \frac{(-1)^n \alpha}{128\pi^3 E_\chi k} \int_{-\infty}^0 dq_0 \frac{q_0 e^{q_0/T_\star}}{e^{q_0/T_\star} - 1} \int dt_E \frac{t_E^n}{\sqrt{t_E - |q_0|^2}} g_0 \left(\frac{\varepsilon_{F,i} - E_i^{t^-}}{q_0} \right) \quad (\text{A.67})$$

where we have substituted $|\bar{\mathcal{M}}|^2 = \alpha t^n$ as the matrix element. Typically, we expect to be in the regime where $g_0 = 1$, and so the differential up-scattering rate is related result for down-scattering through

$$\frac{d\Gamma_{\text{up}}^-}{dq_0} = \frac{e^{-|q_0|/T_\star}}{e^{-|q_0|/T_\star} - 1} \frac{d\Gamma_{\text{down}}^-}{dq_0} \quad (\text{A.68})$$

This result applies generally to all matrix elements, not just the ones $\propto t^n$. The result can be derived from the principle of detailed balance, and hence is true for all interactions we consider. To calculate the total interaction rate, the t_E integrations can be performed in the same manner as in the previous section, with the q_0 integration bounds being $(-\infty, 0)$.

A.4 Non-degenerate weak field limit

When setting up the centre of mass energy interval in section 1.3, we have set the DM energy to 0 at infinity. This means that when taking the classical non-relativistic limit, the interaction rate would approach

$$\Omega^-(r) \rightarrow n_i(r)v_{esc}(r)\sigma, \quad (\text{A.69})$$

in the simple case of a constant cross-section. Taking Eq. 1.39, one can first strip out the Pauli blocking term $(1 - f_{\text{FD}})$, and then the integration in t and s can be performed analytically. Taking the limit $u_i \rightarrow 0$, $E_i = m_i/\sqrt{1 - u_i^2}$, and then the weak field approximation $B(r) \rightarrow 1 - v_{\text{esc}}^2(r)$, for a constant cross-section $\frac{d\sigma}{d\cos\theta_{\text{cm}}} = \frac{\sigma}{2}$, we find

$$\Omega^-(r) \rightarrow m_i^2 \frac{\sigma}{2} \frac{2u_i v_{\text{esc}}(r) f_{\text{FD}}(E_i, r)}{\pi^2} dE_i \quad (\text{A.70})$$

$$= m_i^3 \frac{\sigma}{2} \frac{2u_i v_{\text{esc}}(r) f_{\text{FD}}(E_i, r)}{\pi^2} u_i du_i \quad (\text{A.71})$$

$$= m_i^3 \frac{\sigma}{2} \frac{v_{\text{esc}}(r) f_{\text{FD}}(E_i, r)}{2\pi^3} d^3 u_i \quad (\text{A.72})$$

$$= \frac{\sigma}{2} \frac{v_{\text{esc}}(r) f_{\text{FD}}(E_i, r)}{2\pi^3} d^3 p. \quad (\text{A.73})$$

Cases with $\sigma \propto t^n$ give similar results. Recall that

$$\frac{2f_{\text{FD}}(E_i)}{(2\pi)^3} d^3 p, \quad (\text{A.74})$$

is the number density of neutron states. Then, following expression in 1.31 we substitute it with the classical number density $n_i(r)$, to obtain the expected classical limit given by Eq. A.69.

A.5 Intermediate DM mass range

The interaction rate in Eq. 1.39 can be rewritten in terms of the DM momentum p_χ , such that

$$\begin{aligned} \Omega^-(r) &= \frac{\zeta(r)}{32\pi^3} \int dt dE_i ds |\overline{M}|^2 \frac{E_i}{2s\beta(s) - \gamma^2(s)} \frac{1}{p_\chi} \frac{s}{\gamma(s)} \\ &\quad \times f_{\text{FD}}(E_i, r)(1 - f_{\text{FD}}(E'_i, r)), \end{aligned} \quad (\text{A.75})$$

where we have also used Eq. 1.51. We first consider the case where the squared matrix element depends only on t , i.e. $|\bar{M}|^2 \propto t^n$, we can straightforwardly perform the integral over t ,

$$\Omega^-(r) = \frac{\zeta(r)}{32\pi^3} \int dE_i ds \bar{g}(s) \frac{E_i \gamma(s)}{2s\beta(s) - \gamma^2(s)} \frac{1}{n+1} \left(\frac{\gamma^2(s)}{s} \right)^n \times \frac{1}{p_\chi} f_{\text{FD}}(E_i, r)(1 - f_{\text{FD}}(E'_i, r)). \quad (\text{A.76})$$

We now assume that either $\mu \gg 1$ or $\mu \ll 1$. In both cases, the integration range for s shrinks to $[s_0 - \delta s, s_0 + \delta s]$, with $\delta s \ll s_0$, and the following simplifications can be made;

$$s_0 = m_i^2 + m_\chi^2 + 2 \frac{E_i m_\chi}{\sqrt{B(r)}} = m_i^2 + m_\chi^2 + 2E_i E_\chi, \quad (\text{A.77})$$

$$\delta s = 2 \sqrt{\frac{1 - B(r)}{B(r)}} m_\chi \sqrt{E_i^2 - m_i^2} = 2p_\chi \sqrt{E_i^2 - m_i^2}, \quad (\text{A.78})$$

$$\frac{\gamma(s)}{2s\beta(s) - \gamma^2(s)} \rightarrow \frac{\sqrt{1 - B(r)}}{2(m_i^2 + m_\chi^2)} = \frac{p_\chi}{2E_\chi(m_i^2 + m_\chi^2)}, \quad (\text{A.79})$$

$$\frac{\gamma^2(s)}{s} \rightarrow \frac{4(1 - B(r))m_\chi^2}{B(r)(1 + \mu^2)} = \frac{4p_\chi^2}{1 + \mu^2}. \quad (\text{A.80})$$

If $g(s)$ is regular in s_0 , we can estimate the integral in s to be $2\delta s$, approximating the integrand as being constant in that range, which gives

$$\Omega^-(r) \sim \zeta(r) \frac{1}{16\pi^3} \frac{\sqrt{E_\chi^2 - m_\chi^2}}{E_\chi(m_i^2 + m_\chi^2)} \left[\frac{4(E_\chi^2 - m_\chi^2)}{1 + \mu^2} \right]^n \int dE_i E_i \sqrt{E_i^2 - m_i^2} \times f_{\text{FD}}(E_i, r)(1 - f_{\text{FD}}(E'_i, r)). \quad (\text{A.81})$$

To perform the integral in E_i , we have to potentially deal with Pauli blocking. However, for $\mu \gg 1$, Pauli blocking is not effective and we can drop the $1 - f_{\text{FD}}$ term to obtain

$$\int_{m_i}^{m_i + \varepsilon_{F,i}(r)} dE_i E_i \sqrt{E_i^2 - m_i^2} f_{\text{FD}}(E_i, r) = \frac{[\varepsilon_{F,i}(r)(2m_i + \varepsilon_{F,i}(r))]^{3/2}}{3} = \pi^2 n_{\text{free}}(r) \quad (\text{A.82})$$

This, together with $\zeta(r)$, result in an overall factor of $\pi^2 n_i(r)$, leaving

$$\Omega^-(r) \sim \frac{n_i(r)}{16\pi} \frac{\sqrt{E_\chi^2 - m_\chi^2}}{m_\chi^2 E_\chi} \frac{1}{n+1} \left[\frac{4(1 - B(r))m_\chi^2}{B(r)(1 + \mu^2)} \right]^n, \quad (\text{A.83})$$

and the capture rate reads,

$$C \sim \frac{1}{4v_\star} \frac{\rho_\chi}{m_\chi^3} \text{Erf} \left(\sqrt{\frac{3}{2}} \frac{v_\star}{v_d} \right) \int_0^{R_\star} r^2 dr n_i(r) \frac{1 - B(r)}{B(r)} \frac{1}{n+1} \left[\frac{4(1 - B(r))m_\chi^2}{B(r)(1 + \mu^2)} \right]^n. \quad (\text{A.84})$$

We can now rewrite these expressions in terms of the cross-section which has been averaged over s ,

$$\langle \sigma(r) \rangle = \left\langle \int dt \frac{d\sigma}{dt} \right\rangle_s = \frac{1}{2\delta s} \int_{s_0 - \delta s}^{s_0 + \delta s} ds \int dt \frac{d\sigma}{dt} \quad (\text{A.85})$$

$$= \frac{1}{64\pi m_\chi^2 m_i^2} \frac{B(r)}{(1 - B(r))} \int dt t^n \quad (\text{A.86})$$

$$= \frac{1}{64\pi m_\chi^2 m_i^2} \frac{B(r)}{(1 - B(r))} \frac{1}{(n+1)} \left[\frac{4(1 - B(r))m_\chi^2}{B(r)(1 + \mu^2)} \right]^{n+1} \quad (\text{A.87})$$

$$= \frac{1}{16\pi (m_i^2 + m_\chi^2)} \frac{1}{(n+1)} \left[\frac{4(1 - B(r))m_\chi^2}{B(r)(1 + \mu^2)} \right]^n, \quad (\text{A.88})$$

which leads to,

$$\Omega^-(r) \sim n_i(r) \langle \sigma(r) \rangle \frac{\sqrt{E_\chi^2 - m_\chi^2}}{E_\chi}, \quad (\text{A.89})$$

$$C \sim \frac{4\pi}{v_\star} \frac{\rho_\chi}{m_\chi} \text{Erf} \left(\sqrt{\frac{3}{2}} \frac{v_\star}{v_d} \right) \int_0^{R_\star} r^2 dr n_i(r) \frac{1 - B(r)}{B(r)} \langle \sigma(r) \rangle. \quad (\text{A.90})$$

From Eq. A.90, we can identify the typical $1/m_\chi$ scaling of the capture rate. This equation also looks very similar to the non-relativistic case, with $1 - B(r)$ playing the role of the escape velocity, $v_{\text{esc}}^2(r)$, and $1/B(r)$ being a relativistic correction.

Turning to the case of s -dependent matrix elements, $|\bar{\mathcal{M}}|^2 = g(\bar{s})t^n$ for \bar{g} some function of s , the result is fairly similar. The main difference is that we must keep all terms in m_i and m_χ , leading to the new substitutions

$$\frac{\gamma(s)}{s^2 - [m_i^2 - m_\chi^2]^2} \sim \frac{\sqrt{1 - B(r)}}{2 \left(m_i^2 + m_\chi^2 + 2m_i m_\chi / \sqrt{B(r)} \right)}, \quad (\text{A.91})$$

$$\frac{\gamma^2(s)}{s} \rightarrow \frac{4(1 - B(r))m_\chi^2}{B(r)(1 + \mu^2) + 2\sqrt{B(r)}\mu}. \quad (\text{A.92})$$

Now when we take the limit as $\varepsilon_{F,n} \rightarrow 0$, the integrand over s can be approximated as a δ -function, resulting in s being fixed to the value of s_0 . As such, we no longer need to average the cross-section over s . The results are

$$\Omega^-(r) \sim \frac{n_i(r)}{16\pi} \frac{\sqrt{E_\chi^2 - m_\chi^2}}{E_\chi (m_i^2 + m_\chi^2 + 2m_i E_\chi)} \frac{\bar{g}(s_0)}{n+1} \left[\frac{4(1-B(r))m_\chi^2}{B(r)(1+\mu^2) + 2\sqrt{B(r)}\mu} \right]^n. \quad (\text{A.93})$$

$$C \sim C_{\text{approx},s} = \frac{4\pi}{v_\star} \frac{\rho_\chi}{m_\chi} \text{Erf} \left(\sqrt{\frac{3}{2}} \frac{v_\star}{v_d} \right) \int_0^{R_\star} r^2 dr n_i(r) \frac{1-B(r)}{B(r)} \sigma(r), \quad (\text{A.94})$$

$$\sigma(r) = \int dt \frac{d\sigma}{dt} = \frac{1}{16\pi \left(m_i^2 m_\chi^2 + 2m_i m_\chi / \sqrt{B(r)} \right)} \frac{\bar{g}(s_0)}{(n+1)} \times \left[\frac{4(1-B(r))m_\chi^2}{B(r)(1+\mu^2) + 2\sqrt{B(r)}\mu} \right]^n. \quad (\text{A.95})$$

A.6 Interaction Rate for Low Energies

Need to consider the case where $T_\chi = E_\chi - m_\chi < \mu_F$, with $0 < q_0 < T_\chi < \varepsilon_{F,i}$. Then the t_E integration limits follow the hierarchy; $t_{\mu^+}^+ \sim t_{\mu^-}^+ \geq t_{\mu^-}^- \sim t_{\mu^+}^- \gtrsim 0$, and $t_{\mu^-}^+ \gg t_E^+ \geq t_E^- \gg t_{\mu^-}^-$. Then the only term in A.54 that remains is the first term, and only the $i=j=1$ term contributes, leaving

$$\Gamma^-(E_\chi) = \sum_{n,m} \frac{(-1)^n \alpha_{n,m}}{128\pi^3 E_\chi k} \int_0^{E_\chi - m_\chi} dq_0 \int_{t_E^-}^{t_E^+} dt_E f_1^{(m,n)}(t_E) \quad (\text{A.96})$$

At first order in q_0 and K_χ , we have the following approximations

$$E_\chi \approx m_\chi \quad (\text{A.97})$$

$$k \approx \sqrt{2m_\chi T_\chi} \quad (\text{A.98})$$

$$t_E^\pm \approx 4m_\chi T_\chi \left[1 - \frac{q_0}{2K_\chi} \pm \sqrt{1 - \frac{q_0}{K_\chi}} \right] \quad (\text{A.99})$$

$$\Gamma^- \approx \sum_{n,m} \frac{(-1)^n \alpha_{n,m}}{128\sqrt{2}\pi^3 m_\chi^{3/2} K_\chi^{1/2}} \int_0^{K_\chi} dq_0 \int_{t_E^-}^{t_E^+} dt_E f_1^{(m,n)}(t_E) \quad (\text{A.100})$$

For single term matrix elements such that $|\overline{\mathcal{M}}|^2 = \alpha_{n,m}(-t)^n s^m$, the correspond-

ing $\Gamma_{n,m}^-$ are

$$\Gamma_{0,0}^- = \frac{\alpha_{0,0}}{120\pi^3 m_\chi} K_\chi^2 \quad (\text{A.101})$$

$$\Gamma_{1,0}^- = \frac{2\alpha_{1,0}}{105\pi^3} K_\chi^3 \quad (\text{A.102})$$

$$\Gamma_{2,0}^- = \frac{4\alpha_{2,0} m_\chi}{63\pi^3} K_\chi^4 \quad (\text{A.103})$$

$$\Gamma_{0,1}^- = \frac{\alpha_{0,1}((m_i + m_\chi)^2 + 2m_\chi \varepsilon_{F,i})}{120\pi^3} K_\chi^2 \quad (\text{A.104})$$

$$\Gamma_{1,1}^- = \frac{2\alpha_{1,1}((m_i + m_\chi)^2 + 2m_\chi \varepsilon_{F,i})}{105\pi^3} K_\chi^3 \quad (\text{A.105})$$

$$\Gamma_{0,2}^- = \frac{\alpha_{0,2}((m_i + m_\chi)^2 + 2m_\chi \varepsilon_{F,i})^2}{120\pi^3} K_\chi^2 \quad (\text{A.106})$$

The $\alpha_{n,m}$ can be obtained at some reference point, taken to be the surface of the NS, from the differential cross-section,

$$\frac{d\sigma}{d \cos \theta_{\text{cm}}} = \frac{\alpha_{n,m}(-t)^n s^m}{32\pi(m_i + m_\chi)^2} \quad (\text{A.107})$$

which gives

$$\sigma_{0,0} = \frac{\alpha_{0,0}}{16\pi(m_i + m_\chi)^2} \quad (\text{A.108})$$

$$\sigma_{1,0} = \frac{\alpha_{1,0}}{32\pi(m_i + m_\chi)^2} t_{max} \quad (\text{A.109})$$

$$\sigma_{2,0} = \frac{1}{3} \frac{\alpha_{2,0}}{16\pi(m_i + m_\chi)^2} t_{max}^2 \quad (\text{A.110})$$

$$\sigma_{0,1} = \frac{\alpha_{0,1}}{16\pi(m_i + m_\chi)^2} s \quad (\text{A.111})$$

$$\sigma_{1,1} = \frac{\alpha_{1,1}}{32\pi(m_i + m_\chi)^2} t_{max} s \quad (\text{A.112})$$

$$\sigma_{0,2} = \frac{\alpha_{0,2}}{16\pi(m_i + m_\chi)^2} s^2 \quad (\text{A.113})$$

where I have used

$$t = -\frac{t_{max}}{2}(1 - \cos \theta_{\text{cm}}) \quad (\text{A.114})$$

$$t_{max} \sim \frac{4m_i^2 m_\chi^2}{(m_i^2 + m_\chi^2)} \frac{1 - B(R_\star)}{B(R_\star)} \quad (\text{A.115})$$

$$s \sim m_i^2 + m_\chi^2 + \frac{2m_\chi(m_i + \varepsilon_{F,i})}{\sqrt{B(R_\star)}} \quad (\text{A.116})$$

$$\sim (m_i + m_\chi)^2 \quad (\text{A.117})$$

Again introducing the correction

$$\zeta = \frac{n_i}{n_{free}} \sim \frac{3\pi^2}{(2m_i\varepsilon_{F,i})^{3/2}} n_i \quad (\text{A.118})$$

Then the interaction rates can be expressed with respect to the surface of the star as

$$\Gamma_{0,0}^-(K_\chi) = \frac{\sqrt{2}}{10} \frac{(1+\mu)^2}{\mu} \frac{m_i}{(m_i\varepsilon_{F,i})^{3/2}} \sigma_{surf} n_i K_\chi^2 \quad (\text{A.119})$$

$$\Gamma_{1,0}^-(K_\chi) = \frac{4\sqrt{2}}{35} \frac{(1+\mu)^2(1+\mu^2)}{\mu^2} \frac{1}{(m_i\varepsilon_{F,i})^{3/2}} \frac{B(R_\star)}{(1-B(R_\star))} \sigma_{surf} n_i K_\chi^3 \quad (\text{A.120})$$

$$\Gamma_{2,0}^-(K_\chi) = \frac{\sqrt{2}}{7} \frac{(1+\mu)^2(1+\mu^2)^2}{\mu^3} \frac{1}{m_i(m_i\varepsilon_{F,i})^{3/2}} \left(\frac{B(R_\star)}{(1-B(R_\star))} \right)^2 \sigma_{surf} n_i K_\chi^4 \quad (\text{A.121})$$

$$\Gamma_{0,1}^-(K_\chi) = \frac{\sqrt{2}}{10} \frac{(m_i(1+\mu)^2 + 2\mu\varepsilon_{F,i})}{\mu(m_i\varepsilon_{F,i})^{3/2}} \sigma_{surf} n_i K_\chi^2 \quad (\text{A.122})$$

$$\Gamma_{1,1}^-(K_\chi) = \frac{4\sqrt{2}}{35} \frac{(m_i(1+\mu)^2 + 2\mu\varepsilon_{F,i})(1+\mu^2)}{\mu^2 m_i(m_i\varepsilon_{F,i})^{3/2}} \frac{B(R_\star)}{(1-B(R_\star))} \sigma_{surf} n_i K_\chi^3 \quad (\text{A.123})$$

$$\Gamma_{0,2}^-(K_\chi) = \frac{\sqrt{2}}{10} \frac{(m_i(\mu+1)^2 + 2\mu\varepsilon_{F,i})^2}{\mu(\mu+1)^2 m_i(\varepsilon_{F,i} m_i)^{3/2}} \sigma_{surf} n_i K_\chi^2 \quad (\text{A.124})$$

The average energy loss per collision is given by

$$\langle \Delta T \rangle = \frac{1}{\Gamma^-} \int_0^{K_\chi} dq_0 q_0 \frac{d\Gamma^-}{dq_0} \quad (\text{A.125})$$

which gives the results

$$\langle \Delta T^{0,0} \rangle = \frac{4}{7} K_\chi \sim \langle \Delta T^{0,1} \rangle \sim \langle \Delta T^{0,2} \rangle \quad (\text{A.126})$$

$$\langle \Delta T^{1,0} \rangle = \frac{5}{9} K_\chi \sim \langle \Delta T^{1,1} \rangle \quad (\text{A.127})$$

$$\langle \Delta T^{2,0} \rangle = \frac{28}{55} K_\chi \quad (\text{A.128})$$

The DM will reach thermal equilibrium with the targets when $K_\chi = T_\star$. There are two stages to this process; one where the interactions are not affected by Pauli blocking which takes N_1 collisions, and the next N_2 collisions where Pauli blocking is in effect. The time it takes for thermalisation to occur is given by the sum of the average times between collisions

$$t_{\text{therm}} = \sum_{n=0}^{N_2} \frac{1}{\Gamma^-(T_n)} \sim \sum_{n=N_1}^{N_2} \frac{1}{\Gamma^-(T_n)} \quad (\text{A.129})$$

where T_n is the DM kinetic energy after n collisions. If Pauli blocking is in effect for the entire process, then T_n is related to the initial kinetic energy, T_0 through

$$T_n = T_0 \left(1 - \frac{\Delta T}{T}\right)^n. \quad (\text{A.130})$$

This result implies the following relation;

$$\frac{T_N}{T_0} = \frac{T_{eq}}{T_0} = \left(1 - \frac{\Delta T}{T}\right)^N \quad (\text{A.131})$$

Then for interaction rates which follow $\Gamma^- \propto (K_\chi)^p$, we have that

$$t_{\text{therm}} \propto \sum_{n=N_1}^{N_2} (T_n)^{-p} \quad (\text{A.132})$$

$$= \frac{1}{T_{N_1}^p} \sum_{n=N_1}^{N_2} \left(\left(1 - \frac{\Delta T}{T}\right)^{-p} \right)^n \quad (\text{A.133})$$

$$= \frac{1}{T_{N_1}^p} \frac{(1 - \Delta T/T)^{p(1-N_1)} - (1 - \Delta T/T)^{-pN_2}}{-1 + (1 - \Delta T/T)^p} \quad (\text{A.134})$$

$$\sim \frac{1}{T_{N_1}^p} \frac{(1 - \Delta T/T)^{-pN_2}}{1 - (1 - \Delta T/T)^p} \quad \text{for } N_2 > N_1 \quad (\text{A.135})$$

$$= \frac{1}{T_{N_1}^p} \left(\frac{T_{eq}}{T_{N_1}} \right)^{-p} \frac{1}{1 - (1 - \Delta T/T)^p} \quad (\text{A.136})$$

$$= \frac{1}{T_{eq}^p} \frac{1}{1 - (1 - \Delta T/T)^p} \quad (\text{A.137})$$